WL-TR-95-4087

CERAMIC BEARING SPECIMEN TECHNOLOGY
ADD-ON PROGRAM: OPTIMIZED CERAMIC BEARING

C. JAMES SHIH and ANDRE EZIS

CERCOM, INC.
1960 WATSON WAY
VISTA CA 92083

JUNE 1995

FINAL REPORT FOR 08/14/93-04/14/95

APPROVED FOR PUBLIC RELEASE; DISTRIBUTION IS UNLIMITED

MATERIALS DIRECTORATE
WRIGHT LABORATORY
AIR FORCE MATERIEL COMMAND
WRIGHT PATTERSON AFB OH 45433-7734

DTIC QUALITY INSPECTED 3

19970130 015

NOTICE

When government drawings, specifications, or other data are used for any purpose other than in connection with a definitely related government procurement operation, the United States Government thereby incurs no responsibility nor any obligation whatsoever; and the fact that the government may have formulated, furnished, or in any way supplied the said drawings, specifications, or other data, is not to be regarded by implication or otherwise as in any manner licensing the holder or any other person or corporation, or conveying any rights or permission to manufacture, use, or sell any patented invention that may in any way be related thereto.

This report is releasable to the National Technical Information Service (NTIS). At NTIS, it will be available to the general public, including foreign nations.

This technical report has been reviewed and is approved for publication.

KARL R. MECKLENBURG, Project Engineer
Nonstructural Materials Branch
Nonmetallic Materials Division

KENT J. EISENTRAUT, Chief
Nonstructural Materials Branch
Nonmetallic Materials Division

FOR THE COMMANDER

CHARLES E. BROWNING, Chief
Nonmetallic Materials Division
Materials Directorate

If your address has changed, if you wish to be removed from our mailing list, or if the addressee is no longer employed by your organization, please notify WL/MLBT, Bldg 654, 2941 P Street, Suite 1, Wright-Patterson AFB OH 45433-7750 to help maintain a current mailing list.

Copies of this report should not be returned unless return is required by security considerations, contractual obligations, or notice on a specific document.

REPORT DOCUMENTATION PAGE

1. AGENCY USE ONLY (Leave blank)	2. REPORT DATE JUN 1995	3. REPORT TYPE AND DATES COVERED FINAL 08/14/93--04/14/95

4. TITLE AND SUBTITLE CERAMIC BEARING SPECIMEN TECHNOLOGY ADD-ON PROGRAM: OPTIMIZED CERAMIC BEARING

6. AUTHOR(S). JAMES SHIH ANDRE EZIS

5. FUNDING NUMBERS
C F33615-92-C-5903
PE 62712
PR 8355
TA 00
WU 01

7. PERFORMING ORGANIZATION NAME(S) AND ADDRESS(ES)

CERCOM, INC.
1960 WATSON WAY
VISTA CA 92083

8. PERFORMING ORGANIZATION REPORT NUMBER

9. SPONSORING/MONITORING AGENCY NAME(S) AND ADDRESS(ES)

MATERIALS DIRECTORATE
WRIGHT LABORATORY
AIR FORCE MATERIEL COMMAND
WRIGHT PATTERSON AFB OH 45433-7734
POC: K. R. Mecklenburg, WL/MLBT, WPAFB OH, 937-255-2465

10. SPONSORING/MONITORING AGENCY REPORT NUMBER

WL-TR-95-4087

11. SUPPLEMENTARY NOTES

12a. DISTRIBUTION/AVAILABILITY STATEMENT

APPROVED FOR PUBLIC RELEASE; DISTRIBUTION IS UNLIMITED

12b. DISTRIBUTION CODE

13. ABSTRACT (Maximum 200 words)

A PARTIALLY STABILIZED SILICON NITRIDE BEARING MATERIAL WITH IMPROVED HARDNESS AND FRACTURE TOUGHNESS IS DEVELOPED, USING A HIGH-RATE LOW-COST PROCESS INVOLVING REACTION BONDING, PRESSURELESS SINTERING AND CONTAINERLESS HOT-ISOSTATIC PRESSING. DURING SINTERING AND HOT-ISOSTATIC PRESSING, ALPHA SILICON NITRIDE, ALPHA TO BETA TRANSFORMATION AND BETA SILICON NITRIDE ACICULAR GRAIN GROWTH PROCESSES OCCUR CONCURRENTLY THROUGH A LIQUID PHASE. THE PARTIALLY STABILIZED SILICON NITRIDE, CONTAINING OPTIMAL AMOUNTS OF "HARD" ALPHA SILICON NITRIDE AND "TOUGH" ACICULAR BETA SILICON NITRIDE, HAVE BOTH HIGH HARDNESS AND FRACTURE TOUGHNESS TO ENHANCE FRICTION AND WEAR PERFORMANCE FOR THE BEARING APPLICATIONS. THIS OPTIMAL MICROSTRUCTURE IS ACHIEVED THROUGH A COMPOSITION AND PROCESS DESIGN.

14. SUBJECT TERMS

SILICON NITRIDE, HARDNESS, FRACTURE TOUGHNESS, PARTIAL STABILIZATION, PHASE TRANSFORMATION, ACICULAR GRAIN GROWTH MICROSTRUCTURAL DEVELOPMENT COMPOSITION, PROCESSING

15. NUMBER OF PAGES 90

16. PRICE CODE

17. SECURITY CLASSIFICATION OF REPORT UNCLASSIFIED	18. SECURITY CLASSIFICATION OF THIS PAGE UNCLASSIFIED	19. SECURITY CLASSIFICATION OF ABSTRACT UNCLASSIFIED	20. LIMITATION OF ABSTRACT SAR

TABLE OF CONTENTS

LIST OF FIGURES

LIST OF TABLES

FOREWORD

This document is a final report covering work performed under an Add-On to U.S. Air Force Systems Command Contract No. F33615-92-C-5903. An interim final report for the original portion of the program (WL-TR-95-4083) was submitted in December 1993. The Air Force Contracting Officer was Roger D. Mullins. The Air Force Project Engineer was Karl R. Mecklenburg of Wright Laboratory/MLBT (513) 255-2465. This project was sponsored by:

Materials Directorate
Wright Laboratory
Air Force Systems Command (ASD)
United States Air Force
Wright Patterson AFB, OH 45433-6533

The Advanced Research Projects Agency, (ARPA) in Arlington, Virginia, was the original source of the funding. The project was based on a Cercom proposal submitted in response to ARPA Broad Agency Announcement (BAA) 91-11-DARPA.

1. INTRODUCTION

The work described in this report was initiated in March of 1992 under a program entitled "Ceramic Bearing Specimen Technology." The original period of performance of this program was to be 18 months. The objective of the program was to develop a processing technology capable of producing high-quality ceramic bearing balls at a high production rate and at competitive cost. The original program successfully achieved its objectives. However, the opportunity to further improve the technology was apparent from some of the experimental findings, and an additional funding increment with an 18 month period of performance was granted. Cercom submitted an interim report (WL-TR-95-4083) for the original portion of the program in December 1993. The present document details the work performed in the "Add-On" portion of the program.

In the original portion of the program, eight different compositions were screened, incorporating different proportions of Si_3N_4, Y_2O_3, TiO_2, and AlN. Parameters related to the seven distinct unit processes involved in the manufacture of the bearing elements were selected during the program. These unit processes were:

1. Powder Blending,

2. Cold Isostatic Pressing,

3. Prenitriding,

4. Green Machining,

5. Nitriding,

6. Sintering, and

7. Hot Isostatic Pressing (HIP),

By the conclusion of the program, the composition consisting of Si_3N_4 - 4% Al_2O_3 - 4% Y_2O_3 - 1% TiO_2 - 3% AlN (4/4/1/3) had been identified as the best composition along with its set of process parameters. The materials produced from this composition and

1

process parameters, designated as Cercom PSO-H, exhibited the mechanical properties listed in Table 1.1.

Table 1.1 Properties of the Material Developed in the Original Program

Material	PSO-H Silicon Nitride
Density	3.24 g/cm^3
Average Flexural Strength	930 MPa (135 Ksi)
Characteristic Flexural Strength	1.01 GPa (146 Ksi)
Weibull Modulus	14
Fracture Toughness	5.9 MPa$\sqrt{m}$ (5.4 Ksi$\sqrt{in}$)
Vickers Hardness	1510 kg/mm^2

During the screening of the compositions and process parameters used during the initial program, a wide variation in mechanical properties was observed. The number of experiments that could be run in the available time period was not sufficient to truly optimize any of the composition or process parameters. By the end of the program, it was clear that the potential for further improvements in properties was very great, if more combinations of parameters could be evaluated. Thus, the add-on program was launched to enable a further refinement of these parameters, especially the composition and the sintering and HIPing conditions.

The objective of the add-on program was to optimize the material composition and processing parameters established in the original program to develop materials of better quality than any other Si$_3$N$_4$ materials now available in the United States. Specifically, the goal was to produce a composition and a set of process parameters resulting in Si$_3$N$_4$ bearing materials which met the following two criteria:

1.   Indentation fracture toughness > 6.0 MPa$\sqrt{m}$

2.   Vickers hardness > 1550 kg /mm^2.

These targets are part of a set of criteria established by a major multinational manufacturer of bearings, and comprise part of the "Class I" specification for ceramic

ball bearings. Meeting the Class I specification is a major milestone toward achieving widespread commercial acceptance of the materials. Other property requirements are also included in the "Class I" specification, such as strength and distribution of pores and inclusions. In Tables 1.2 and 1.3, the requirements for pores and inclusions in Class I, II, and III bearing materials are listed. This is a very detailed set of criteria based on many years of experience with experimental ceramic bearing materials in which failure probabilities were correlated to microstructural features. Figure 1.1 illustrates the hardness and fracture toughness criteria defining the three classes of bearing materials.

Table 1.2 Maximum Limits for Microstructural Features of Each Material Class Compared with Cercom PSO-H Developed in the Original Program.

Microstructure Feature		Material Class Limit			Cercom PSO-H		
		I	II	III	Ball Lot 1	Ball Lot 2	Rod Lot
Porosity:	- Volume %	0.02	0.06	0.06	0.02	0.02	0.04
	- Size (μm)	10	10	25	10	10	10
Metallic Phases:	- Volume %	0.2	0.6	0.6	0.02	0.6	0.6
	- Size (μm)	10	10	25	10	10	10
Ceramic 2nd Phases:	- Volume %	0.2	0.6	0.6	<.02	<.02	<.02
	- Size (μm)	25	25	25	10	10	10

Table 1.3 Maximum Number of Inclusions per cm^2 of Cross-Section Compared with Cercom PSO-H Developed in the Original Program.

Size of Inclusion (μm)	Material Class Limits			Cercom Material		
	I	II	III	Ball Lot 1	Ball Lot 2	Rod Lot
200 -	0	0	1	0	0	0
100 - 200	0	1	2	0	0	0
50 - 100	1	2	4	0	0	0
25 - 50	4	8	16	0	1	0
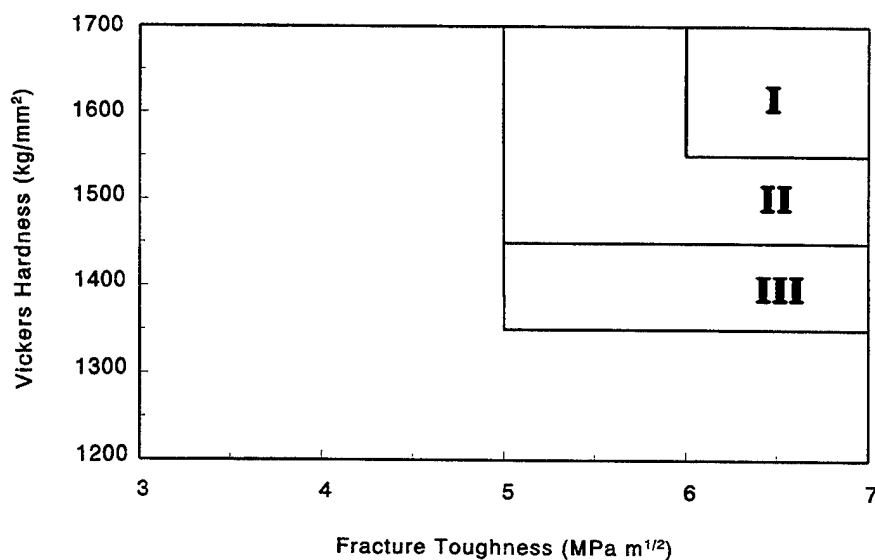
Figure 1.1   *Hardness and Fracture Toughness Requirements for Silicon Nitride Bearing Materials.*

By the conclusion of the original portion of this development program, all the Class I criteria were met by the down-selected Cercom material (PSO-H), except for hardness and toughness. These two parameters just barely failed to meet the Class I limits. Currently, no ceramic bearing materials manufactured anywhere in the United States meet the Class I specification. The program results suggested that the Class I category was within reach of the technology base established in our program, and so the add-on program was initiated in an effort to further improve the material to meet all of the Class I criteria. A "Class I" designation would make the Cercom material competitive with the best foreign-made Si_3N_4 bearing balls.

The add-on program employed the principles of statistical design of experiment to process a large array of different material compositions and sets of process parameters to develop an optimum microstructure. The choices of material compositions were guided by our growing understanding of the control of the α/β Si_3N_4 phase ratio within the finished material to optimize its hardness and toughness.

Si_3N_4 has two structural modifications: α and β. α-Si_3N_4 has a much higher hardness than its β counterpart, and the α-Si_3N_4 converts to β-Si_3N_4 at high temperatures. The β-Si_3N_4 occurs as a mixture of acicular and equiaxed grains. Increasing the content of acicular β-Si_3N_4 increases the fracture toughness. An optimum balance between "hard" α- and "tough" acicular β-Si_3N_4 needs to be found to simultaneously maximize hardness and fracture toughness.

During this add-on program, Cercom learned how to control this balance through a selection of additive composition and processing conditions using a "partial stabilization" approach. This approach involved stabilizing a fraction of α-Si_3N_4 for hardness and promoting the acicular grain growth of β-Si_3N_4 for fracture toughness during sintering and HIPing processes. By the conclusion of this add-on program, both a composition and a set of processing parameters were identified which consistently resulted in a Class I Si_3N_4 bearing material.

BLANK PAGE

2. BACKGROUND AND TECHNICAL APPROACH

Rolling element bearings for use at high speeds or in extreme environments require a bearing material exhibiting light weight, high strength, and good corrosion and wear resistance. Hardness and fracture toughness are usually listed as desired properties, especially for a ceramic bearing material. A material having a high hardness usually exhibits good wear resistance, and a ceramic having a high fracture toughness is often considered reliable. A combination of high hardness and fracture toughness leads to better bearing surface finish and resistance to damage from foreign particles and impacts.

Silicon nitride is considered as the best ceramic material for use in high performance bearings. However, the material was originally developed for high temperature structural applications. A brief history of silicon nitride development is summarized in Table 2.1[1]. In the last 40 years, the material development was concentrated in near-shape fabrication, grain boundary engineering for high temperature properties, and acicular grain growth for high fracture toughness and high strength. The need for the combination of high hardness and fracture toughness was never realized.

Table 2.1 History of Silicon Nitride Development[1].

1896	Synthesis of Si_3N_4	Germany
Late 1950s	Near Shaped Reaction Bonded Si_3N_4	UK
Early 1960s	Liquid Phase Sintering for Hot Pressed Si_3N_4	UK
Early 1970s	Nitridation Kinetics for Improved Reaction Bonded Si_3N_4	USA
Early 1970s	Grain Boundary Engineering for High Temperature Properties	USA
Mid 1970s	Over-pressure Sintered Si_3N_4	USA, Japan
Late 1970s	Glass-Encapsulation Hot Isostatic Pressed Sintered Si_3N_4	Sweden
Late 1970s	Two Step Gas Pressure Sintered Si_3N_4	USA, Japan
1980s	Applications and Commercialization	Japan
1990s	Self-Reinforced Si_3N_4 for High Toughness and High Strength	USA, Japan

The objective of this add-on program was to develop a silicon nitride bearing material with improved hardness and fracture toughness to enhance friction and wear performance, using a high-rate low-cost process involving reaction bonding, pressureless sintering and containerless hot isostatic pressing. This add-on program optimized composition and microstructure to achieve both high hardness and fracture toughness.

2.1   Optimization of Composition

Because of its strong covalent bonding and low atomic diffusivity, silicon nitride cannot be densified without sintering additives. Additives, such as Y_2O_3 and Al_2O_3, react with the surface SiO_2 to form a liquid for liquid phase sintering. The types and amounts of additives affect not only the grain growth of Si_3N_4 but also the development of the intergranular phase. However, the trends for hardness and fracture toughness are usually opposite. For example, it has been noted that hardness decreases and fracture toughness increases with increasing amounts of Y_2O_3, as shown in Figure 2.1[2]. To achieve high hardness and high toughness, the composition must be optimized.
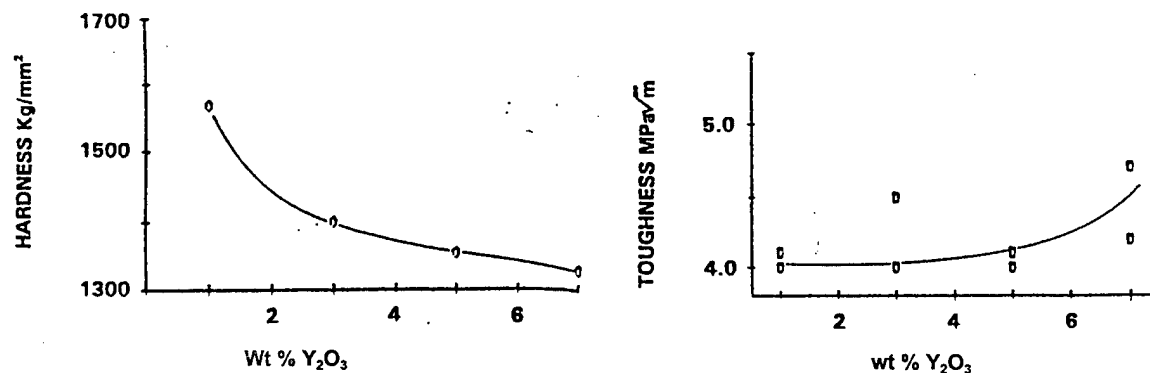
Figure 2.1   *Effect of Y_2O_3 on Hardness and Fracture Toughness[2].*

The intergranular phase is derived from the liquid phase and can be either crystalline or amorphous, depending on the additive composition and the processing conditions. Since silicon nitride bearing materials are made up of Si_3N_4 crystals and an

intergranular phase, the degree of crystallinity of the intergranular phase is expected to influence both hardness and fracture toughness. In addition, the composition of the intergranular phase may also affect properties. For example, the hardness and fracture toughness of Y-Si-Al-O-N oxynitride glasses are determined by the nitrogen content, as shown in Figure 2.2[3]. Two important aspects are noted from this composition effect:

1. Both hardness and fracture toughness of an oxynitride glass can be increased by increasing the nitrogen content. Some additives, such as AlN, may be incorporated into the oxynitride phase, resulting in an increase in the nitrogen content.

2. Oxynitride glasses have much lower hardness and fracture toughness than Si_3N_4. An improvement in both hardness and fracture toughness in a silicon nitride body can be expected if the total amount of the intergranular phase is reduced.
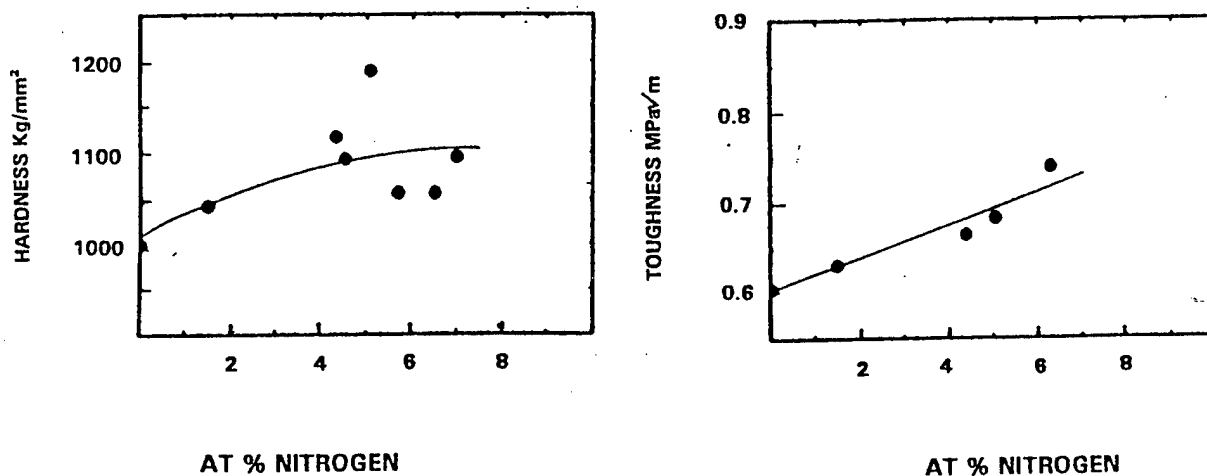
Figure 2.2   *Effect of Nitrogen Content on Hardness and Fracture Toughness of Oxynitride Glasses[3].*

TiO_2 is one of the additives used in the original program. TiO_2 not only provides oxygen as an "oxygen pump" to assist densification, but also coverts to hard *in situ-*

formed TiN, leading to hardening. In the original program, we noted that a small amount of TiO_2 can promote the acicular Si_3N_4 grain growth, as shown in Figure 2.3. However, with an extra 2% of TiO_2, the material showed a dramatic decrease in hardness, most likely because of an induced change in the composition of the intergranular phase. Therefore, an optimization of TiO_2 content was necessary.
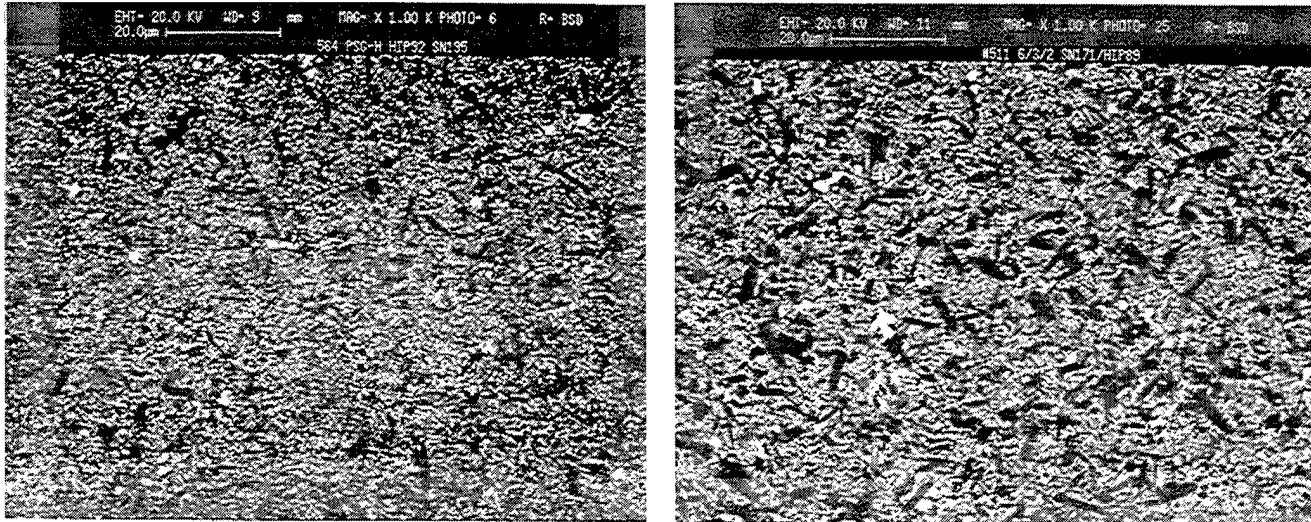
Composition	6% Y_2O_3 + 3% Al_2O_3	Composition	6% Y_2O_3 + 3% Al_2O_3 + 2% TiO_2
Hardness	1450 kg/mm²	Hardness	1310 kg/mm²
Toughness	5.6 MPa $\sqrt{m}$	Toughness	5.9 MPa $\sqrt{m}$
Intergranular Phase	Oxynitride Glass	Intergranular Phase	Oxynitride Glass

Figure 2.3   Effects of TiO_2 on Microstructure and Properties.

2.2   Optimization of Microstructure

Grain size of a material always affects its mechanical properties. The effects of grain size on hardness and fracture toughness are shown in Figure 2.4[4,5]. The hardness is decreased with increasing grain size[4], following the Hall-Petch relationship for plastic flow:

where G is the grain size in μm. Fracture toughness of a polycrystalline ceramic is usually dependent on various microstructural and chemical effects, such as aspect ratio of acicular β-Si_3N_4 grains, fracture resistance of the grain boundary regions, and residual stresses. However, fracture toughness appears to increase with increasing grain size[5]. The results suggest the following relationship:

$$K_{IC} = 1.6 + 2.8\,(G)^{1/2} \quad MPa\,\sqrt{m}$$

To achieve both high hardness and fracture toughness, the grain size must be optimized.
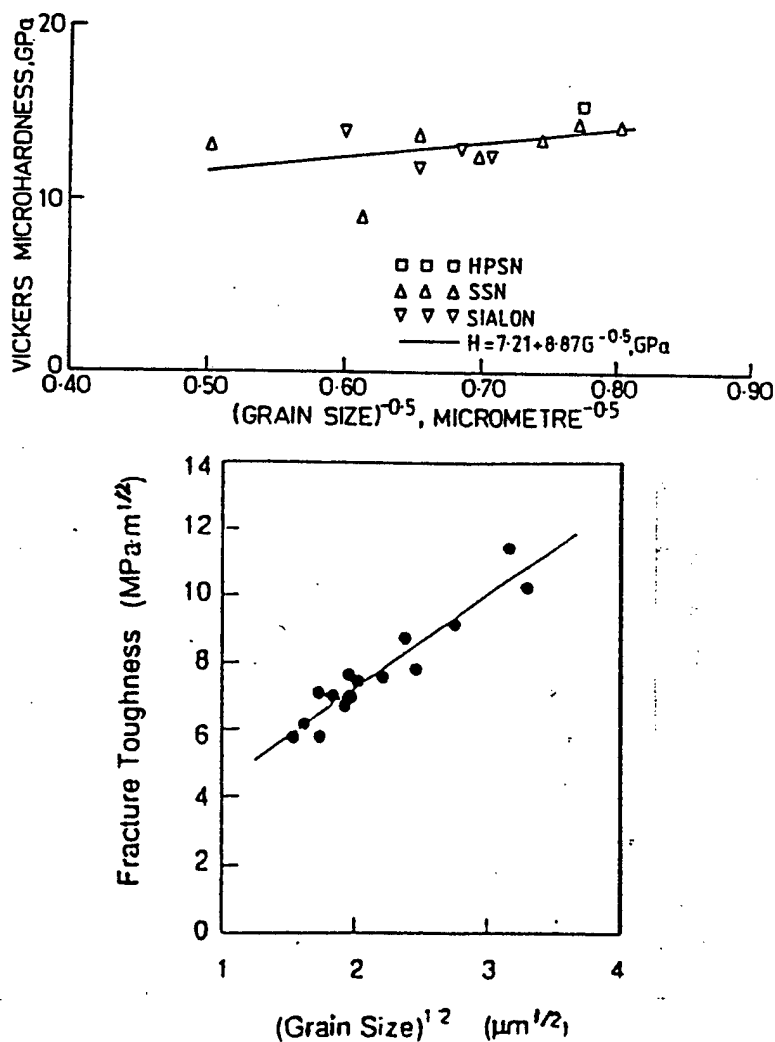
Figure 2.4   Effects of Grain Size on Hardness and Fracture Toughness.[4,5]

11

Grain size is always influenced by the processing conditions. The effects of HIPing temperature on hardness and fracture toughness are shown in Figure 2.5[6]. While increasing the HIPing temperature, the grain size would be inevitably increased, resulting in a reduction in hardness and an increase in fracture toughness. Therefore, grain size optimization must be accompanied by a processing optimization.
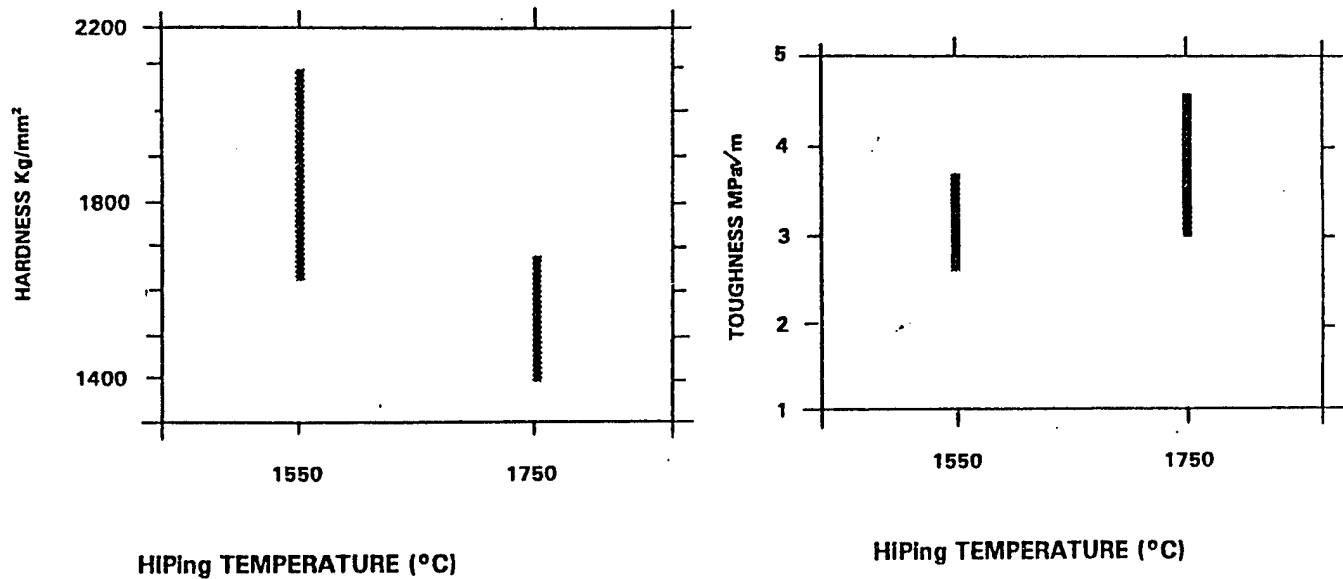
Figure 2.5 *Effects of Processing Temperature on Hardness and Fracture Toughness[6].*

Properties of a silicon nitride bearing material can also be tailored via a control of Si_3N_4 crystal structures. Si_3N_4 occurs in two different structural modifications: α and β. The differences in structure and properties between these two modifications are listed in Table 2.2. α-Si_3N_4 is usually considered to be a low temperature phase and converts to β-Si_3N_4 at high temperatures through a dissolution-precipitation mechanism. Nevertheless, the α-Si_3N_4 can be retained through a stabilization process. α-Si_3N_4 has two large interstitial sites in the crystal lattice, and an α-Si_3N_4 crystal can be stabilized if the interstitial sites are occupied by other atoms, such as Y and Yb. The stabilizing atoms must have appropriate charges and comparable sizes to fit into these interstitial

sites. Since Y_2O_3 is one of our sintering additives, it can provide the necessary stabilizing atoms.

As shown in Table 2.2, α-Si_3N_4 has a higher hardness but lower fracture toughness than β-Si_3N_4. β-Si_3N_4 occurs as a mixture of acicular and equiaxed grains. Increasing the content of acicular β-Si_3N_4 increases the fracture toughness. A silicon nitride material with an optimal balance of "hard" α- and "tough" acicular β-Si_3N_4 can exhibit both high hardness and fracture toughness. A tailored microstructure can be achieved through a control in the α stabilization, $\alpha \rightarrow \beta$ transformation and β-Si_3N_4 acicular grain growth processes. Since all processes are carried out in a liquid phase and are diffusion controlled reactions, the additive composition and processing temperatures must be selected appropriately to achieve the optimal balance of "hard" α- and "tough" acicular β-Si_3N_4.

Table 2.2 Difference in α and β Si_3N_4.

	α Si_3N_4	β Si_3N_4
Crystal Structure	Hexagonal	Hexagonal
Lattice Parameter (Angstrom)	a = 7.76	a = 7.60
	c = 5.62	c = 2.91
Space Group	P31c	$P6_3$
Atomic Packing	2 Large Interstitial Sites	Closed Packing, Less Strained
Thermal Stability	Low Temp Phase	High Temp Phase
Grain Morphology	Equiaxed	Acicular and Equiaxed
Hardness (kg/mm^2)	1900-2100	1400-1600
Fracture Toughness (MPa $\sqrt{m}$)	2 - 5	4 - 7

2.3   Technical Approach

The overview of the add-on program is shown in Figure 2.6. The program was divided into four tasks, involving two composition iterations and a processing

optimization. All available data were reviewed and analyzed to establish a program strategy and to select 25 candidate compositions (Task 1). Specimens were fabricated and characterized to evaluate the causes and effects between hardness, fracture toughness and the compositions (Task 2). Promising compositions were selected and a new set of compositions was evaluated for confirmation (Task 3). Processing optimization for the final composition was performed for fabricating optimized bearing blanks (Task 4).

Task 1

Selection of
Candidate Compositions

↓

Task 2

Fabrication and Characterization
of Specimens
(1st Iteration)

↓

Task 3

Selection of
Promising Compositions
(2nd Iteration)

↓

Task 4

Processing Optimization
Blank Fabrication
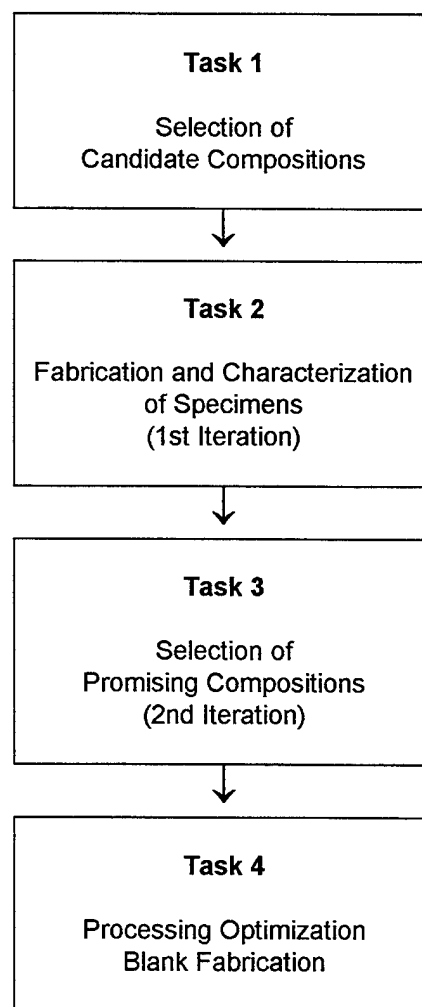
Figure 2.6   *Overview of the Add-On Program.*

3. MATERIALS AND PROCEDURES

Cercom has selected a sintered reaction bonded silicon nitride (SRBSN) process starting with Si, Y_2O_3, Al_2O_3, TiO_2, and AlN for the fabrication of silicon nitride bearing blanks. The constituent unit processes are:

1. Powder Blending,
2. Cold Isostatic Pressing,
3. Prenitriding,
4. Green Machining,
5. Nitriding,
6. Sintering, and
7. Hot Isostatic Pressing (HIP)

Each of these unit processes was studied as a separate task within the original programand and was documented in the interim report (WL-TR-95-4083). The results were directly applied to the material fabrication in this add-on program.

3.1   Powder Blending

Powder blending is carried out by ball-milling. Weighed portions of ceramic powders and a liquid vehicle are added to a neoprene-lined steel jar, typically of 8.7 liter (2.3 gallon) capacity. Silicon nitride balls are also added to the jar to fill about 40% of its volume. The powder slurry/grinding media mixture is sealed into the jar, and the jar is rolled on its side for a period of time, typically one to two days. The viscosity of the slurry may be measured by interrupting the rolling and immersing the probe of a Brookfield viscometer into the jar. If the viscosity is outside the range of 300 to 500 centipoise, then more liquid or powder may be added to bring the viscosity within this range, which is most conducive to efficient milling.

At the completion of ball-milling, the slurry is poured into a pan and placed in an oven to drive off the liquid. A common addition to this process is to filter the slurry

before it flows into the pan to remove any particles larger than 40 μm or any agglomerates which were not broken up and dispersed during ball milling. When the liquid has all evaporated, the powder is left in the form of a cracked cake. The cake is placed into a dry milling jar with balls and milled for 1 or 2 hours to break up the cake. The resulting powder is sifted through 5 and 30 mesh sieves, and collected in a plastic bag.

3.2   Cold Isostatic Pressing

The blended powders are formed into a solid compact or *"green body"* by cold isostatic pressing or *"isopressing"*. In this process, the powder is poured into a shaped rubber bag, which is sealed, immersed in water, and subjected to hydraulic pressurization for a few seconds. The resulting part possesses sufficient strength to be handled without breaking, and the shape established by isopressing will be retained through the nitride reaction bonding process.

The isostatic press used in this work was manufactured by Autoclave Engineering, Inc. It has a 30.5 cm (12 in.) diameter by 91.4 cm (36 in.) deep working chamber. Its maximum pressure capacity is 207 MPa (30,000 psi). The device is shown on the right side of the photograph in Figure 3.1.
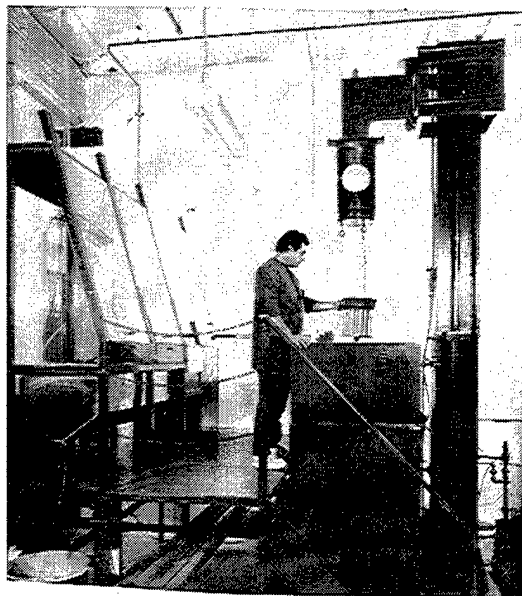
Figure 3.1   *Cercom's Cold Isostatic Press.*

3.3 Prenitriding

Prenitride is an isothermal heat treatment to increase the strength of the isopressed rods so that they could be efficiently machined in a high-speed centerless grinder. The rods produced in the cold isostatic press are too weak to be ground economically.

Prenitriding and nitriding involve the same process. The only difference between these two is that, in prenitriding, the process is interrupted after a few hours, so only a fraction of the silicon in the part is converted to silicon nitride. The strength of the prenitrided rods is determined by the amount of conversion. The more conversion, the stronger the rods are. However, if the conversion is too high, the resulting rods would be very difficult to grind, because of their high strength and hardness.

The optimum prenitriding treatment results in a 4% weight gain. This weight gain would be controlled by temperature and cycle time. The weight gain comes from the reaction between the silicon and nitrogen. The 4% weight gain can be achieved by running the furnace long enough to consume the nitrogen gas corresponding to the weight gain in the parts. As a result, the actual length of time depends on the quantity of material loaded into the furnace and the temperature.

Prenitriding is carried out in a cold-walled vacuum furnace shown in Figure 3.2. All interior materials of construction are selected for their overall inertness. Heating elements, hearth and heat shield are fabricated from molybdenum, and high-purity alumina is used for electrical insulation. The cold-compacted parts are placed in Si_3N_4 containers with cover plates and are stacked within the furnace hot zone. The furnace vessel is evacuated to out-gas the green ware and construction materials. Gas back-filling is used to assist this procedure. Once the system integrity is confirmed by a leak check, the temperature is raised to 600°C (1112°F) and held until a vacuum of 10^{-3} torr or lower is established. This procedure assists the outgassing process and removes all chemically-combined water and residual volatiles associated with the system. The

17

furnace is then back-filled with nitrogen and is maintained at a pressure of 121 kPa (2.9 psig). The prenitriding is carried out at 1125°C (2060°F) and the progress of reaction is monitored by metering the quantity of nitrogen that flows into the furnace.

After the prenitride process consumes the nitrogen required to provide isopressed rods 4% weight gain, the process is terminated by cooling the furnace to room temperature.
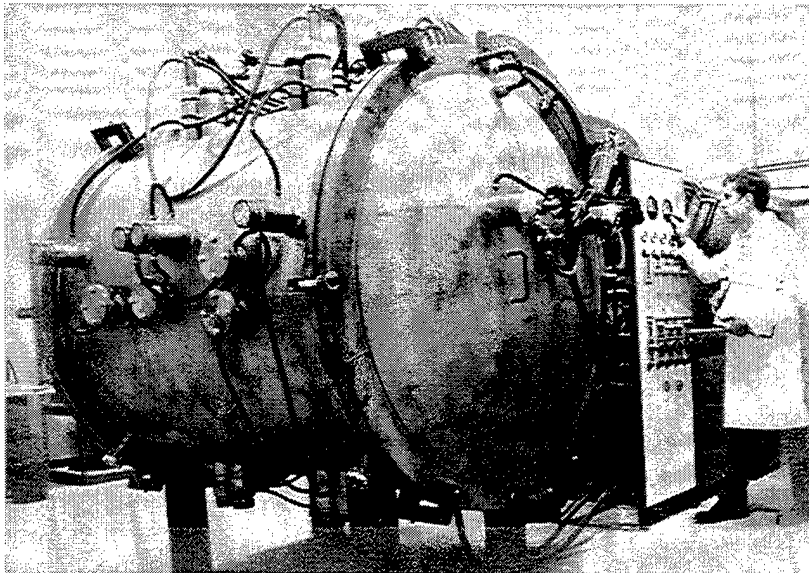
Figure 3.2   *A Cercom-designed Cold-walled Vacuum Furnace for Prenitriding and Nitriding.*

3.4   Green Machining

A centerless grinder is used to grind the green-formed and prenitrided rods to a uniform diameter. The term "centerless" refers to the fact that this type of grinder does not require the axis of the rod to be carefully centered in the machine, as in a lathe. The rod is laid between two rotating cylinders; one cylinder does the grinding, while the other keeps the part counter-rotating against the grinding wheel. This centerless grinder design is also capable of cutting a rod into a set of spheres, using a specially shaped grinding wheel.

Cercom uses a centerless grinder manufactured by the Glebar Company. This grinder can be adapted to mass production with special automatic feed attachments, making it capable of producing up to 1400 balls per hour. Photographs of the Glebar grinder and the special ball-grinding wheel are shown in Figures 3.3 and 3.4, respectively.
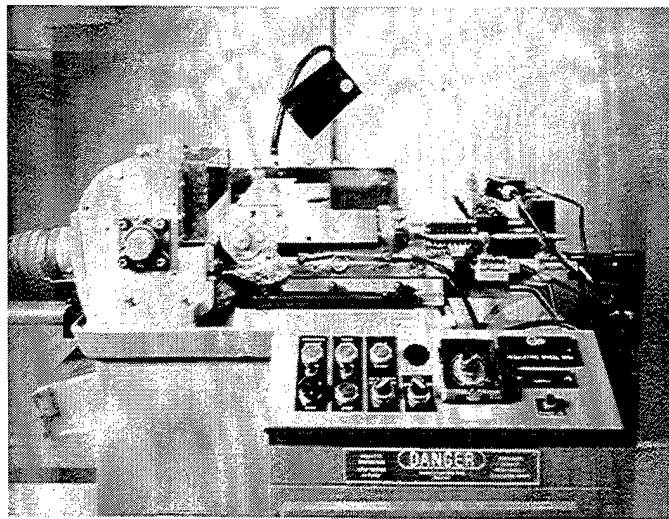
Figure 3.3   *Glebar Centerless Grinder used by Cercom to Grind Rods and Balls.*
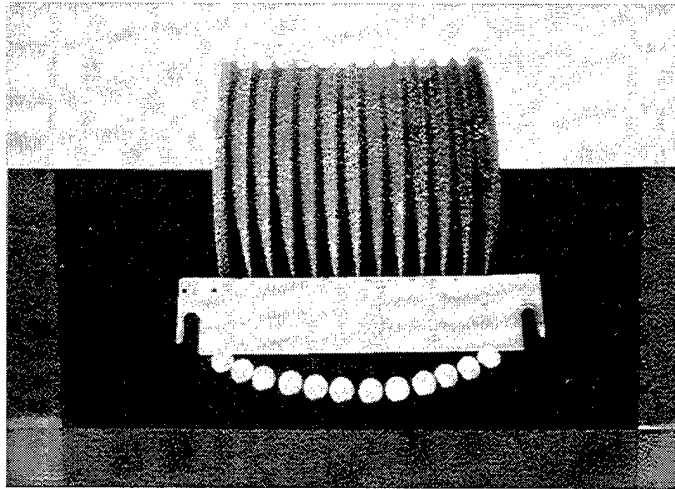
Figure 3.4 *Special Grinding Wheel used in the Centerless Grinder for Producing Balls from Rods.*

3.5   Nitriding - Reaction Bonding

After green machining, the parts are returned to the nitriding furnace to convert the silicon in the parts to silicon nitride completely. Nitriding is carried out in the same cold-walled vacuum furnace as for the prenitriding as, shown in Figure 3.2. The green-machined parts are placed in Si_3N_4 containers with cover plates and are stacked within the furnace hot zone. The furnace vessel is evacuated to out-gas the green ware and construction materials. Gas back-filling is used to assist this procedure. Once the system integrity is confirmed by a leak check, the temperature is raised to 600°C (1112 °F) and held until a vacuum of 10^{-3} torr or lower is established. This procedure assists the outgassing process and removes all chemically-combined water and residual volatiles associated with the system. The furnace is then back-filled to a pressure of 121 kPa (2.9 psig) with a gas containing 3 percent H_2, 25 percent He, and 72 percent N_2 is maintained for the remainder of the cycle. The conversion process takes place in the temperature range of 1100°C (2012°C) to 1400°C (2552°F) with two principal nitriding reactions:

$$3\ Si\ (s) + 2\ N_2\ (g) \rightarrow Si_3N_4$$

$$3\ Si\ (g) + 2\ N_2\ (g) \rightarrow Si_3N_4$$
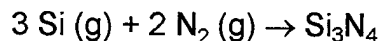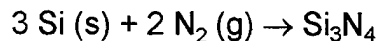
Successful nitriding is achieved by precise control over the highly exothermic nature of these reactions. The kinetics at a given temperature produce an initial rapid nitriding rate which slows until an essentially complete reaction asymptote is reached (Arrhenius curve). The accepted technique for exothermic management is to proceed incrementally, beginning at 1100°C through the nitriding temperature range. At each temperature increment, the nitriding rate is allowed to reach its asymptote level before the temperature is again increased.

The progress of the nitriding reaction is monitored by metering the quantity of nitrogen that flows into the furnace. The gas is delivered by a "demand system" that introduces a metered volume of gas, and then monitors furnace gas pressure. When this pressure drops below a specified level, another increment of gas is injected. The atmospheric control system keeps a count of the number of increments, and the time interval between increments. When the nitrogen demand drops below a predetermined rate, then the temperature is increased. Continuing this process to the maximum nitriding temperature of 1400°C will result in full conversion of the silicon to silicon nitride. The time required at a given temperature for the reaction rate to reach the asymptote level is dependent upon many variables. Some of the most critical variables are Si metal purity, surface area and particle size, compact green density and cross-sectional thickness. If management of the exotherm is not precise, the kinetics will cascade and the heat generated by the reaction will cause melting of the silicon. Once melted, the silicon coalesces and cannot be nitrided. The duration of a complete nitriding cycle is approximately ten days, including initial outgassing and post-nitride cool-down.

3.6 Sintering

Sintering is conducted in a pressureless (ambient pressure) furnace specially-constructed by Cercom. This furnace uses graphite heating elements and graphite felt

insulation within a steel vacuum chamber. The maximum part size it can accommodate is 305 cm diameter and 76 cm high. The part is placed in the sintering furnace inside low-density silicon nitride retorts. The retorts serve to create a localized atmosphere that maintains a gas-phase equilibrium that prevents loss of SiO from the parts and associated silicon nitride decomposition. This controlled environment also keeps carbon species away from the part, preventing silicon carbide formation. In the sintering of silicon nitride parts, the furnace is pumped down to a vacuum of 1 torr, and then back-filled with inert gas. A photograph of the sintering furnace is shown in Figure 3.5.
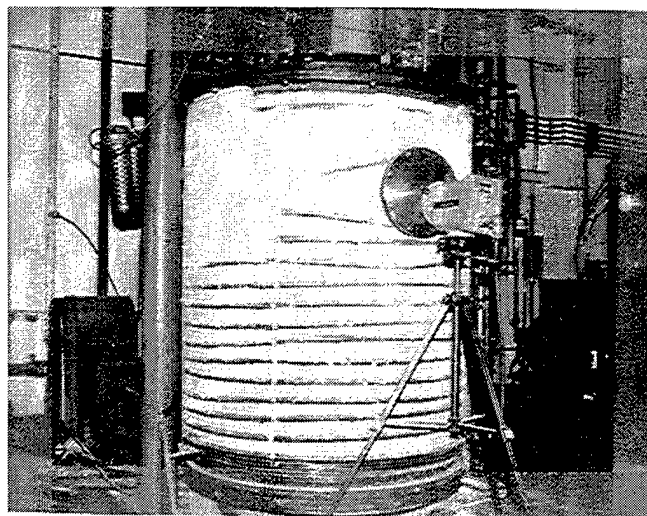
Figure 3.5   *Cercom's Sintering Furnace.*

3.7   Hot Isostatic Pressing (HIPing)

Hot Isostatic Pressing or HIP processing of ceramic materials traditionally involves vacuum encapsulation of a part before subjecting it to high-pressure gas in a heated pressure vessel. The encapsulant or container is a temperature and pressure resistant material that serves as a pressure-transmitting membrane during processing. This process has been studied extensively and has been applied successfully to silicon nitride by a number of manufacturers. Theoretically dense isotropic bodies are

22

produced with significant improvements in physical properties and overall material reliability (Weibull modulus > 12). Furthermore, it has been recently shown that, using the encapsulation HIP techniques, silicon nitride can be densified to better than 95% of theoretical density using no sintering aids a significant advance in Si_3N_4 processing.

The encapsulation HIP process, although effective and quite versatile, is a high-cost process because of the expense involved with preparing and removing the container material. Additionally, the contact surface of processed components can show chemical variation to significant depths within the part due to diffusion between the container and the part being HIPed. The outer layer of affected material must be removed by diamond grinding and, therefore, the process detracts considerably from the concept of "net shaping". Processing parts with sharp edges and corners represents a serious problem if the part must be encapsulated.

Cercom and others have developed an alternate HIP process technique known as "sinter-HIP", or sometimes referred to as "containerless HIPing" because of the positive economic gains that may be realized by eliminating the encapsulation process. Sinter-HIP processing is generally accomplished by using two separate thermal treatments. The first includes pressureless sintering of an RBSN part to a closed porosity state. Closed porosity with a density greater than 90 percent of theoretical density is required so that the surface of the article can act as the pressure-transmitting membrane. The second treatment uses HIPing to remove all residual porosity from the sintered article to achieve theoretical density.

In theory, the sinter-HIP process should remove all residual porosity and produce a theoretically dense body. However, in practice, the application of this process to Si_3N_4 is not straightforward. Major technical issues include: (a) minimum density requirements of the sintered material, (b) solubility of Ar and N_2 gas (used to supply pressure) into the silicon nitride intergranular phase, and (c) vaporization of the liquid phase. During containerless HIPing, the temperature must be high enough to

23

form a liquid phase, but low enough to prevent Si_3N_4 sublimation. In addition, the partial pressure of N_2 should be controlled to eliminate the gas dissolution-evolution and vaporization reactions. We have demonstrated that the minimum required sintered density is 95%. Results from our original program suggested use of high temperature (>1775°C) and low pressure (< 69 MPa [10,000 psi]) during the containerless HIPing operation.

4.0 RESULTS AND DISCUSSION

4.1 Selection of Candidate Compositions

The technical challenge of this add-on program was to achieve high hardness (>1550 kg/mm^2) and high fracture toughness(>6.0 MPa $\sqrt{m}$) concurrently. The strategy for optimizing composition and microstructure to accomplish the technical objectives relied on the following guidelines:

- The hardness depends on the grain size and the volume fraction of Si$_3$N$_4$.

- The fracture toughness depends on microstructural and micro-mechanical effects, viz. on the size of acicular β-Si$_3$N$_4$ grains, the fracture resistance of the grain boundary regions, and residual stresses.

- The hardness is composition dependent whereas, the fracture toughness is microstructure dependent.

The approach we adopted was first to establish the compositions satisfying the hardness requirement and then to manipulate the microstructure to maximize the fracture toughness. Before designing an experimental matrix of new compositions to evaluate, an analysis of previous work was conducted to assess the influence on hardness from each of the constituents.

4.1.1 Linear Regression Analysis of Previous Work

We evaluated eight different compositions during the original program. A linear regression method was employed to analyze the relationship between the hardness and compositions. The analytical method assumed that each constituent had a linearly independent contribution to the overall hardness of the material. It assumed no interactions between ingredients. These assumptions were clearly oversimplifications of how hardness was affected, but in the absence of any other methods to predict

hardness, it proved to be quite useful, nonetheless. The linear regression model can be formulated in the following expression:

$$[HARDNESS] = [COMPOSITION] \times [A]$$

Basically, there are five components, in terms of additives. They are Si_3N_4, Y_2O_3, Al_2O_3, TiO_2 and AlN. Eight compositions, 6/3/2, 8/2/2, 8/1/2, 5/2/3, 4/4/1/3, 4/7/1, 8/2 and 6/3 (with numerical designations representing weight percent of Y_2O_3, Al_2O_3, TiO_2 and AlN, respectively), were studied in the original program. Because of the degrees of freedom, it was decided to use only the first 5 compositions to calculate the regression matrix and to use the last 3 compositions to evaluate the validity of such analysis. The whole calculation was therefore based on the following equation:

Si_3N_4	Y_2O_3	Al_2O_3	TiO_2	AlN					Hardness	
89	6	3	2	0		A1			H	6/3/2
88	8	2	2	0		A2			H	8/2/2
89	8	1	2	0	X	A3	=		H	8/1/2
90	5	2	3	0		A4			H	5/2/3
88	4	4	1	3		A5			H	4/4/1/3

where: A1 is the coefficient of regression for Si_3N_4

A2 is the coefficient of regression for Y_2O_3

A3 is the coefficient of regression for Al_2O_3

A4 is the coefficient of regression for TiO_2

and   A5 is the coefficient of regression for AlN.

Ai can be considered as the "contribution" from the ith component.

It is understood that all processing conditions can influence the properties. Therefore, this regression analysis grouped parts together from the same HIP cycles. It was assumed that the processing steps occurring before HIPing were reproducible and

identical. The results of the matrix algebra solutions to the regression equation are given in Table 4.1. Results for the five regression coefficients are given for six different HIP runs.

Table 4.1 Calculation of Hardness Regression Coefficients

Run No	1	2	3	4	5	6	AVERAGE
HIP Temp °C	1875	1875	1750	1750	1825	1825	
Press MPa	6.9	3.45	3.45	6.9	3.45	3.45	
HIP Time Min	30	75	30	75	75	75	
Gas	Ar/N_2	Ar/N_2	Ar/N_2	Ar/N_2	N_2	Ar/N_2	
A1 (Si_3N_4)	16.26	20.76	14.55	14.83	15.6	14.59	16.1 ± 2.4
A2 (Y_2O_3)	-1.24	-24.24	10.55	9.33	5.1	9.59	1.5 ± 13.4
A3 (Al_2O_3)	-6.74	-28.24	9.55	3.83	-9.4	5.59	-4.2 ± 13.8
A4 (TiO_2)	-8.24	-96.24	13.55	6.33	3.1	24.59	-9.5 ± 43.9
A5 (AlN)	34.42	-11.24	25.55	29.66	41.77	52.26	28.7 ± 21.7

The coefficients given in the "average" column can then be used to predict hardness using the following formula:

$$H_V = 16.1[Si_3N_4] + 1.5[Y_2O_3] - 4.2[Al_2O_3] - 9.5[TiO_2] + 28.7[AlN] \quad kg/mm^2$$

The higher the value of each coefficient, the larger the contribution made by that constituent to the overall hardness. To test the validity of the model thus developed, these coefficients were used to predict the hardnesses of the three compositions omitted from the initial calculations. These predictions are compared to actual measured hardness values in Table 4.2. The calculations were made using the coefficients derived separately for each HIP run, not with the averaged values.

In a larger demonstration of the usefulness of the linear model, all of the measured hardness data from eight compositions and six HIP runs were plotted against the predicted values for each point. The resulting graph is shown in Figure 4.1. The graph shows a uniform scatter band of about ± 3 % across the entire range of

hardnesses measured, so despite the simplicity of the model, its predictive value appears to be very good.

The close correspondence between predicted and measured values using this model is remarkably good. It should now be possible to predict the hardness of any combination of additives before the material is ever produced. A major result of this analysis is that aluminum nitride (AlN), with a hardness coefficient of 28.7, appears to have the greatest influence on hardness of any of the additives. This suggests that future experimental compositions ought to include larger amounts of this compound, and perhaps smaller amounts of TiO_2 and Al_2O_3, which have negative contribution to hardness.

Table 4.2 Comparison of Predicted vs. Measured Hardness Values

Run No.		Vickers Hardness (Kg/mm^2)			
		1	2	3	4
H 4/7/1	Calculated	1371	1436	1403	1376
	Measured (Error Δ)	1366 (0.37%)	1419 (1.2%)	1395 (.57%)	1344 (2.4%)
H 8/2	Calculated	1440	1618	1413	1417
	Measured (Error Δ)	1414 (1.8%)	1427 (13.4%)	1401 (0.8%)	1408 (0.6%)
H 6/3	Calculated	1452	1659	1416	1417
	Measured (Error Δ)	1474 (1.5%)	1490 (11.3%)	1451 (2.4%)	1440 (1.6%)
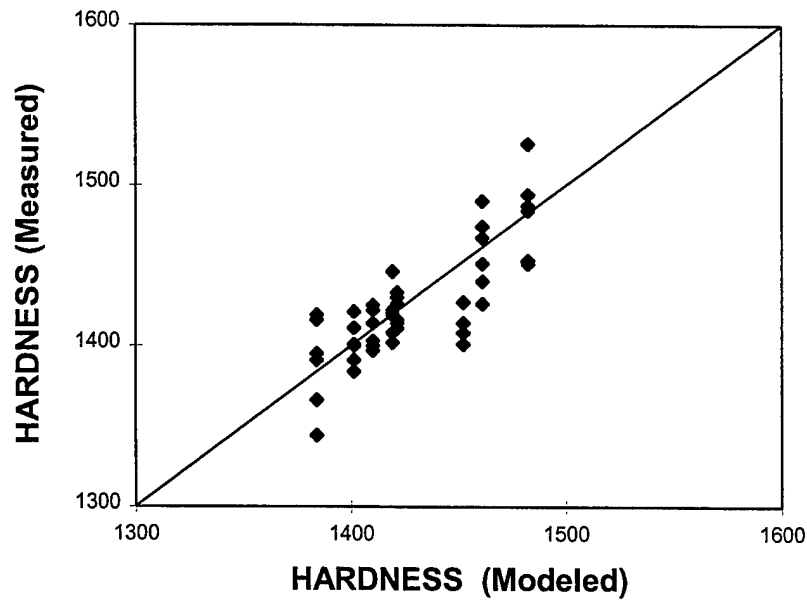
Figure 4.1   *Comparison of Measured Hardness Data (in kg/mm²) Against Modeled Data (in kg/mm²) from the Linear Regression.*

4.1.2   First Iteration Experimental Design and Processing

An array of 25 different additive formulations was designed for the first iteration of fabrication and characterization experiments to be carried out under the add-on program. The 25 compositions are listed in Table 4.3.

Table 4.3 Additive Compositions for the First Iteration

Group	Composition No.	Composition $(Y_2O_3/Al_2O_3/TiO_2/AlN)$ in wt. %
A	1	4/4/1/3
B	2	4/3/2/3
	3	4/2/3/3
	4	4/1/4/3
	5	4/5/0/3
C	6	4/3/1/4
	7	4/2/1/5
	8	4/1/1/6
	9	4/0/1/7
D	10	1/1/0.25/0.75
	11	2/2/0.5/1.5
	12	3/3/0.75/2.25
	13	6/6/1.5/4.5
E	14	4/0/0/2
	15	4/1/1/4
	16	4/2/2/6
	17	6/0/1/6
	18	6/1/2/2
	19	6/2/0/4
	20	8/0/2/4
	21	8/1/0/6
	22	8/2/1/2
F	23	4/4/1/3/20 (ultrafine Si_3N_4)
	24	4/4/1/3/40 (ultrafine Si_3N_4)
G	25	4/4/1/3 (small Si)

The compositions listed in the table are divided into groups based on the rationales for selection of formulations. These rationales are explained below:

A. Use 4/4/1/3 as the baseline composition. This was the optimum composition which was developed in the original program.

B. Vary the ratio of Al_2O_3/TiO_2, holding all else constant. Both Al_2O_3 and TiO_2 function as "oxygen pumps" for densification. As described in Section 2.1, we have observed a positive contribution of TiO_2 on acicular grain growth of β-Si_3N_4. This group of compositions was designed to evaluate the effect of different "oxygen pumps".

C. Vary the oxygen/nitrogen ratio by varying the ratio of Al_2O_3/AlN, holding the other additives at the baseline levels. The chemistry of the intergranular phases can influence properties of silicon nitride (see Section 2.1). The addition of AlN was expected to increase the nitrogen content in the intergranular phase.

D. Vary the total amount of the additives, while keeping the relative proportions equal to the baseline composition. Since the intergranular phases usually have lower hardness and toughness than Si_3N_4 crystals (see Section 2.1), reducing the total amount of additives was expected to increase both hardness and toughness.

E. Expand the composition range, using a partial factorial array, based on a three-level factorial test plan as described in Table 4.4.

Table 4.4 Three-Level Factorial Test Plan in the First Iteration

Factors	Level		
	1	2	3
Y_2O_3	4 %	6 %	8 %
Al_2O_3	0 %	1 %	2 %
TiO_2	0 %	1 %	2 %
AlN	2 %	4 %	6 %

To carry out a test plan with four factors at three levels each would require 4^3 (64) compositions. A partial factorial pattern was used to select a more manageable number of samples, in this case 9, from the 64 sample compositions. The results of the linear regression analysis were directly

applied to design this experimental matrix. As described in Section 4.1.1, AlN and Y_2O_3 had a positive contribution, while Al_2O_3 and TiO_2 were detrimental to the hardness. The amount of each additive in this experimental matrix was selected so that high hardness could be expected.

F. Determine the effects of nucleation/growth seeding on microstructure. This composition group has a fifth number in the composition descriptor, corresponding to the weight percent of an ultrafine (0.2 µm) silicon nitride powder additive. This powder was added as a "seed" to reduce the average grain size of the finished material. As described in Section 2.2, grain size has a significant influence on hardness and fracture toughness. Cercom has observed some dramatic property improvements from this approach in other silicon nitride development work done outside this program.

G. Determine the effects of a fine particle size of silicon powder (Grade 2F, 1.5 µm average particle size) as a substitute for the standard silicon powder (Grade 2E, 3.5 µm average particle size). It was expected that fine starting raw material could result in a small grain size for Si_3N_4. The baseline composition was still used.

4.2   Fabrication and Characterization of Specimens (First Iteration)

4.2.1 Fabrication of Specimens from the First Iteration

The 25 compositions listed in Table 4.3 were processed through powder blending, cold isostatic pressing, nitriding, pressureless sintering and hot isostatic pressing. Fabrication procedures are described in Section 3. The prenitriding step was not necessary for specimen fabrication in this stage of the program since no green machining was performed. All the powder blends were compacted into rods by cold isostatic pressing. Numbers were scratched into the surface of each rod to maintain traceability throughout the process. All the rods were weighed and loaded into a controlled atmosphere furnace to nitride silicon to silicon nitride.

Weight change of each composition in the nitride reaction is listed in Table 4.5. In theory, a silicon part would increase in weight by 66% in the process of being converted to silicon nitride, based on the stoichiometric relationship. In practice, a weight gain of no more than 60% can be realized in a pure silicon part, because some of the nitriding occurs in the gas phase and forms silicon nitride that condenses away from the part. When SRBSN materials are nitrided, they contain additives, such as Y_2O_3 and Al_2O_3, which do not take up nitrogen, so that the weight gains for these materials are determined by the additive composition. The minimum acceptable weight gain is calculated based on the 60% nitrogen take-up in silicon for each composition. As shown in Table 4.5, the actual weight gain was higher than the minimum acceptable weight gain for all compositions; therefore, the nitride reaction was concluded to be successful.

Table 4.5 Weight Change on Nitriding and α-Si_3N_4 Content in Nitrided Parts

Group	#	Y_2O_3	Al_2O_3	TiO_2	AlN	Si_3N_4	Actual Wt Gain %	Minimum Acceptable Wt Gain %	$\alpha/(\alpha+\beta)$ %
A	1	4	4	1	3	0	52.7	49.5	25
B	2	4	3	2	3	0	52.7	49.7	30
B	3	4	2	3	3	0	52.5	49.9	35
	4	4	1	4	3	0	52.9	50.1	28
	5	4	0	5	3	0	52.3	50.4	27
C	6	4	3	1	4	0	53.1	49.5	38
	7	4	2	1	5	0	52.8	49.5	48
	8	4	1	1	6	0	52.8	49.5	42
	9	4	0	1	7	0	50.6	49.5	64
D	10	1	1	0.25	0.75	0	60.8	57.2	70
	11	2	2	0.5	1.5	0	57.1	54.6	50
	12	3	3	0.75	2.25	0	54.6	52.0	40
	13	6	6	1.5	4.5	0	47.6	44.7	30
E	14	4	0	0	2	0	57.1	54.4	55
	15	4	1	1	4	0	54.4	51.1	54
	16	4	2	2	6	0	50.8	48.0	49
	17	6	0	1	6	0	51.9	48.6	42
	18	6	1	2	2	0	52.1	50.5	41
	19	6	2	0	4	0	53.0	49.3	53
	20	8	0	2	4	0	50.4	48.0	48
	21	8	1	0	6	0	49.6	46.8	65
	22	8	2	1	2	0	51.3	48.6	41
F	23	4	4	1	3	20	37.5	34.4	23
	24	4	4	1	3	40	27.1	22.1	20
G	25	4	4	1	3	0	51.1	49.5	34

34

The nitride process takes place in the temperature range of 1100 to 1400°C. Both α- and β-Si_3N_4 are formed during the nitride process. The formation of α-Si_3N_4 is associated with a nitride reaction of silicon solid and silicon vapor; whereas, the growth of β-Si_3N_4 occurs with the presence of liquid. Impurities, such as Fe and Al, usually promote β-Si_3N_4 formation at the end of the nitride cycle. Additives may form a low temperature eutectic liquid, resulting in the promotion of β-Si_3N_4 formation. The phase content of all 25 nitrided parts was characterized using XRD, as listed in Table 4.5. Results suggested that the α to β ratio in nitrided parts was strongly influenced by the composition of the additives and starting powders. Some qualitative assessments are summarized as follows:

1. The Al_2O_3/TiO_2 ratio did not affect the α content. (Group B)

2. An increase in AlN tended to increase the α content. (Group C)

3. The α content decreased with an increase in the total amount of additives. (Group D)

4. TiO_2 had a dominant contribution, over other additives, in determining the phase content in Si_3N_4. The more TiO_2 addition, the less α-Si_3N_4 was formed. (Group E)

5. Ultra-fine Si_3N_4 powder did not affect the α phase content. (Group F)

6. Smaller Si powder tended to have higher amounts of α-Si_3N_4. (Group G)

Densification conditions always affect the microstructure and the concomitant properties. After nitriding, all 25 compositions went through four different sintering + HIPing cycles. Sintering was conducted in a pressureless (ambient pressure) furnace. The furnace used graphite heating elements and graphite felt insulation within a steel vacuum chamber. The part was placed in the sintering furnace inside a silicon nitride retort. The retort served to create a localized atmosphere to maintain a gas phase equilibrium, preventing loss of SiO from the parts. HIPing was performed in a graphite

hot-isostatic-pressing furnace. The partial pressure of N_2 and total pressure were controlled to prevent the sublimation of Si_3N_4 and to eliminate the gas dissolution-evolution process (Section 3.6). The temperatures for sintering and HIPing are listed in Table 4.6. The sintering time was 10 hours for every run. HIPing time was 75 minutes in the first three conditions, and condition No. 4 was HIPed for 150 minutes.

Table 4.6 Processing Conditions for the First Iteration

Condition	Sintering Temperature (°C)	HIPing Temperature (°C)	Description
1	1700	1875	Low Temperature Sintering and Low Temperature HIPing
2	1700	1950	Low Temperature Sintering and High Temperature HIPing
3	1750	1950	High Temperature Sintering and High Temperature HIPing
4	1700	1875 + 1950	Long HIPing

Density was measured using a water absorption method (ASTM C-373). As shown in Table 4.7, all compositions, except No. 10, reached full density under all four processing conditions. The composition No. 10 had very low amounts of additives; as a result, the material did not have a sufficient liquid phase for densification.

4.2.2 Characterization of Specimens from the First Iteration

The processing steps in the first iteration resulted in 100 different material samples, representing 25 compositions and four sets of heat treating conditions (sintering + HIPing). The compositions and processing conditions are listed in Tables 4.3 and 4.6, respectively. Every material was characterized in terms of hardness and fracture toughness. Both hardness and fracture toughness were measured using the Vickers indentation technique.

Table 4.7 Density of Specimens from the First Iteration

		Cycle No. Sinter Temp °C HIP Temp °C	1 1700 1875	2 1700 1875	3 1750 1950	4 1700 1875+1950
	No.	Composition	Density g/cm^3	Density g/cm^3	Density g/cm^3	Density g/cm^3
A	1	4/4/1/3	3.23	3.23	3.23	3.23
B	2	4/3/2/3	3.24	3.25	3.24	3.24
	3	4/2/3/3	3.26	3.26	3.25	3.25
	4	4/1/4/3	3.27	3.27	3.27	3.27
	5	4/0/5/3	3.28	3.28	3.28	3.27
C	6	4/3/1/4	3.24	3.23	3.24	3.24
	7	4/2/1/5	3.23	3.24	3.24	3.24
	8	4/1/1/6	3.24	3.24	3.24	3.24
	9	4/0/1/7	3.24	3.24	3.24	3.24
D	10	1/1/0.25/0.75	2.89	2.93	2.95	2.83
	11	2/2/.5/1.5	3.21	3.21	3.20	3.21
	12	3/3/.75/2.25	3.22	3.22	3.22	3.22
	13	6/6/1.5/4.5	3.25	3.25	3.25	3.25
E	14	4/0/0/2	3.23	3.23	3.23	3.23
	15	4/1/1/4	3.24	3.23	3.24	3.24
	16	4/2/2/6	3.25	3.25	3.25	3.24
	17	6/0/1/6	3.27	3.26	3.26	3.27
	18	6/1/2/2	3.27	3.27	3.27	3.27
	19	6/2/0/4	3.26	3.25	3.25	3.25
	20	8/0/2/4	3.30	3.30	3.29	3.30
	21	8/1/0/6	3.28	3.28	3.28	3.28
	22	8/2/1/2	3.29	3.29	3.28	3.28
F	23	4/4/1/3/20	3.22	3.23	3.23	3.23
	24	4/4/1/3/40	3.23	3.23	3.23	3.23
G	25	4/4/1/3 Fine	3.24	3.24	3.24	3.23

In addition to hardness and toughness measurements, many of the samples were also examined by SEM and x-ray diffraction to characterize the microstructures. Grain size and phase content were quantified in these microstructural analyses.

4.2.2.1 Hardness, Toughness and Correlation to Additive Contents

Measured hardness and toughness data from the first iteration materials are listed in Table 4.8. All hardness and toughness values are plotted in Figure 4.2. There were two data points that fell into the Class I region. They both had the same composition (6/0/1/6) and they were processed under conditions Nos. 2 and 3.

Hardness and toughness appeared to be influenced by the processing temperatures. Materials processed under the lowest sintering and HIPing temperatures (condition No. 1) had the highest average hardness and lowest average toughness. This difference in hardness and toughness was attributed to the grain size effect. Low processing temperatures would lead to small grain size, resulting in high hardness and low fracture toughness.

Table 4.8 Hardness and Fracture Toughness of Specimens from the First Iteration

		Cycle No. Sinter °C HIP °C	1 1700 1875		2 1700 1950		3 1750 1950		4 1700 1875+1950	
	No.	Composition	H_v kg/mm^2	K_{IC} MPa√m	H_v kg/mm^2	K_{IC} MPa√m	H_v kg/mm^2	K_{IC} MPa√m	H_v kg/mm^2	K_{IC} MPa√m
A	1	4/4/1/3	1475	5.80	1410	6.22	1443	6.28	1443	6.41
B	2	4/2/3/3	1446	5.78	1374	6.39	1368	6.77	1428	6.34
	3	4/3/2/3	1486	5.92	1391	6.44	1375	6.46	1422	6.10
	4	4/1/4/3	1423	5.27	1374	6.46	1383	6.94	1374	6.34
	5	4/0/5/3	1408	5.85	1392	6.82	1381	6.94	1383	6.49
C	6	4/3/1/4	1517	5.09	1473	5.15	1438	5.22	1444	5.91
	7	4/2/1/5	1567	4.98	1524	4.55	1511	4.58	1494	5.42
	8	4/1/1/6	1658	5.33	1544	4.32	1573	4.35	1556	4.37
	9	4/0/1/7	1527	5.13	1498	5.73	1458	5.53	1451	5.68
D	11	2/2/.5/1.5	1510	5.26	1466	6.25	1442	5.80	1447	6.09
	12	3/3/.75/2.25	1517	5.33	1471	6.10	1451	6.26	1447	6.36
	13	6/6/1.5/4.5	1509	5.00	1425	6.44	1445	6.34	1456	5.96
E	14	4/0/0/2	1544	4.73	1481	6.09	1497	6.23	1475	4.97
	15	4/1/1/4	1531	5.18	1509	5.77	1454	5.66	1472	5.42
	16	4/2/2/6	1555	4.75	1514	5.72	1492	5.71	1472	5.59
	17	6/0/1/6	1641	5.39	1592	6.06	1582	6.63	1538	5.34
	18	6/1/2/2	1456	5.44	1412	6.39	1406	6.15	1408	6.28
	19	6/2/0/4	1585	5.73	1505	4.57	1498	3.26	1541	5.43
	20	8/0/2/4	1497	5.62	1406	6.12	1444	6.36	1425	6.48
	21	8/1/0/6	1652	5.09	1579	5.70	1612	5.54	1565	5.16
	22	8/2/1/2	1475	5.03	1406	5.23	1395	4.32	1415	5.63
F	23	4/4/1/3/20	1517	5.44	1423	6.57	1437	6.31	1437	6.34
	24	4/4/1/3/40	1497	5.24	1427	6.39	1427	6.31	1432	6.24
G	25	4/4/1/3 Fine	1493	5.62	1405	6.31	1427	6.25	1419	6.24
	All	Average Std. Dev.	1520 48	5.33 0.27	1458 55	5.91 0.54	1456 48	5.84 0.70	1456 39	5.86 0.46
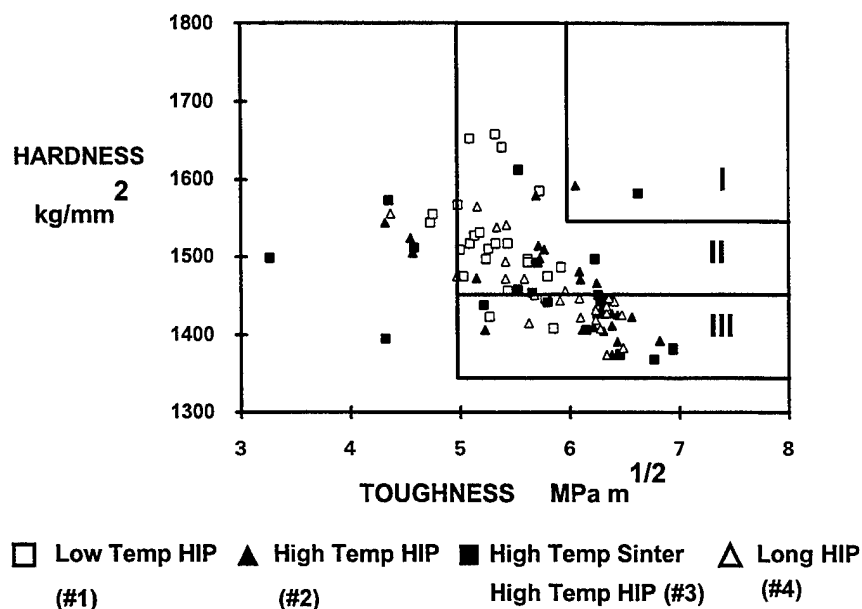
Figure 4.2 *Hardness and Toughness of Specimens from the First Iteration.*

Both measured hardness and toughness were also influenced by the composition of additives and starting powders. As described in Section 4.1.2, composition No. 1, which was developed in the original program, served as a baseline in this iteration. All compositions were divided into groups based on the rationales for selection of formulations. Correlation of properties to additive content can provide an insight to the contribution of each component. Since there were four different processing conditions in this iteration, the average of the properties of each composition was used to elucidate the causes and effects in the correlation analysis.

4.2.2.1.1   Effect of the Ratio of Al_2O_3 to TiO_2 (Group B)

Both Al_2O_3 and TiO_2 function as "oxygen pumps" for densification. This group of compositions was designed to evaluate the influence of Al_2O_3 and TiO_2. Results indicated that hardness increased but toughness decreased with increasing the Al_2O_3/TiO_2 ratio, as shown in Figures 4.3 and 4.4. As described in Section 2.2, we observed a positive contribution of TiO_2 to the acicular grain growth of β-Si_3N_4 to enhance the fracture toughness, but TiO_2 reduced the hardness. The results from this study seemed to confirm the finding from the original program. However, since the

variations in hardness and fracture toughness are only about 5%, it was concluded that Al_2O_3 and TiO_2 are equivalent "oxygen pumps" in this study.
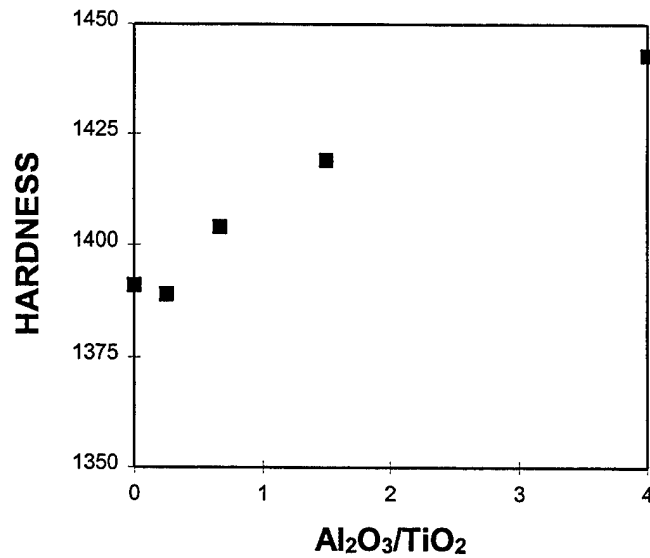
Figure 4.3   *Hardness (in kg/mm²) of the Compositions in the Group Designed to Vary the Ratio of Al_2O_3 to TiO_2.*
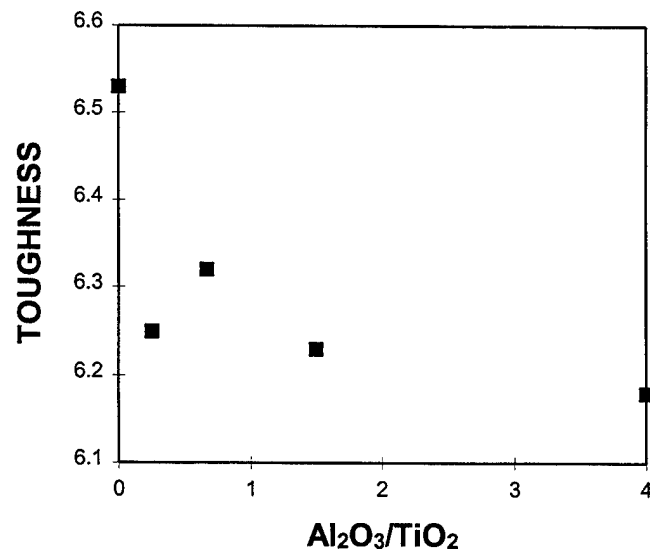
Figure 4.4   *Influence of the Al_2O_3 to TiO_2 Ratio on Fracture Toughness (in MPa $\sqrt{m}$).*

4.2.2.1.2   Effect of the Ratio of Al_2O_3 to AlN (Group C)

The chemistry of the intergranular phase can influence the hardness and toughness of the silicon nitride body. The addition of AlN was expected to increase the nitrogen content in the intergranular phase. Overall, the hardness increased and the toughness decreased significantly as the amount of AlN increased, as shown in Figures 4.5 and 4.6. Results showed that small variation of the Al_2O_3/AlN ratio can lead to a 10% to 30% difference in properties. Therefore, we concluded that the amount of AlN was critical for developing a material with superior hardness and fracture toughness. However, this trend did not apply to the material without Al_2O_3 additive, e.g. the 4/0/1/7 composition. The exception is attributed to a deviation in the development of α-Si_3N_4 microstructure, discussed in Section 4.2.3.
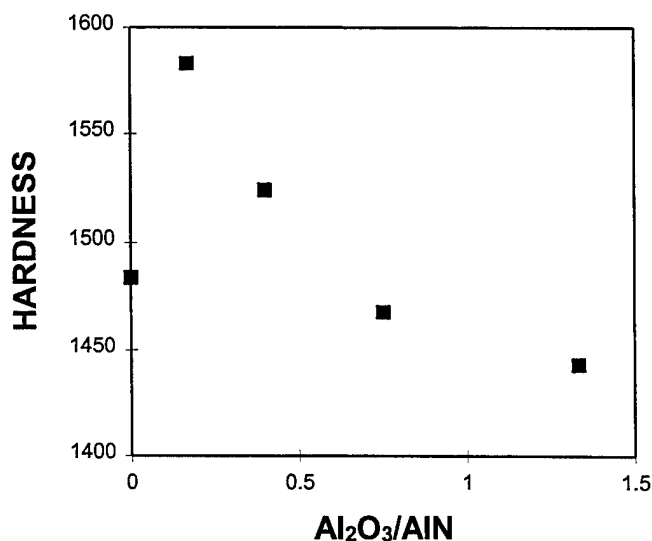
Figure 4.5   *Effect of the Ratio of Al_2O_3 to AlN on Hardness (in kg/mm^2).*
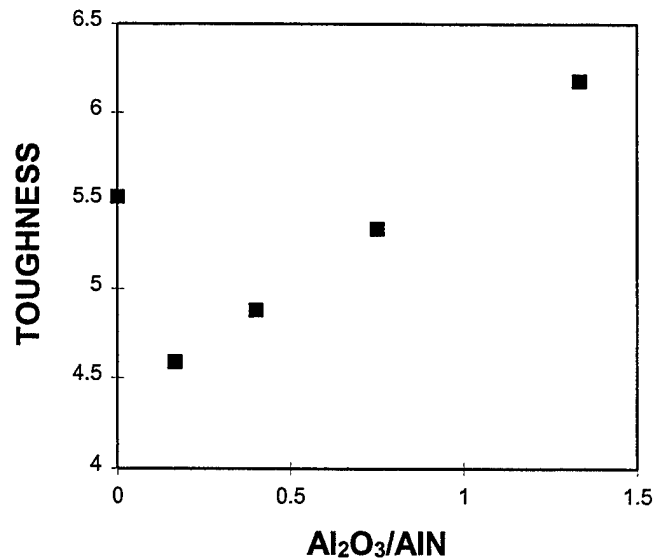
Figure 4.6   Effect of the Ratio of Al_2O_3 to AlN on Fracture Toughness (in MPa $\sqrt{m}$).

4.2.2.1.3   Effect of Total Amount of Sintering Additives (Group D)

In general, the intergranular phases have lower hardness and toughness than Si_3N_4 crystals. It was expected that both hardness and fracture toughness would be improved by decreasing the total amount of the intergranular phase, which is ultimately determined by the total amount of additives. However, as shown in Figures 4.7 and 4.8, hardness did not vary significantly, and the toughness was not improved by reducing the total amount of additives.
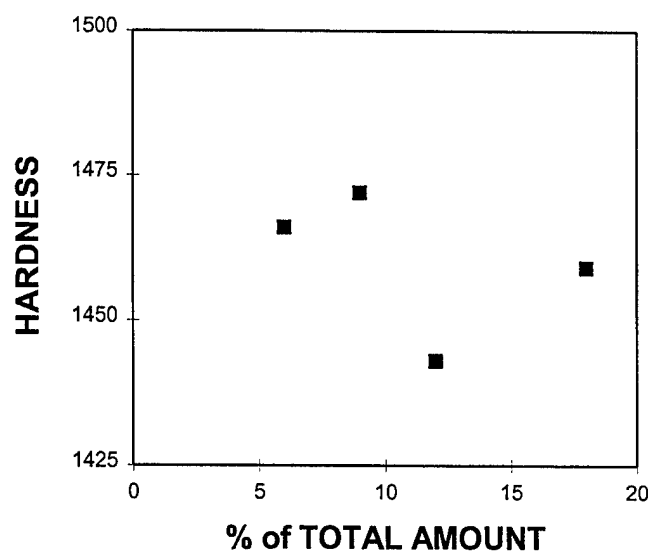
Figure 4.7 *Effect of Total Amount of Sintering Additives on Hardness (in kg/mm².*).
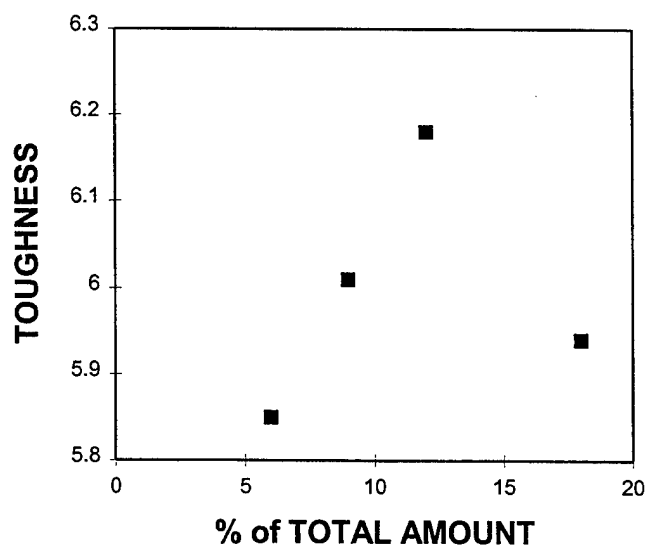
Figure 4.8 *Effect of Total Amount of Sintering Additives on Fracture Toughness (in MPa $\sqrt{m}$).*

43

4.2.2.1.4   Analysis of the Partial Factorial Design of Experiment (Group E)

A four-factor, three-level experiment array was included as one of the composition groups in the first iteration. The "responses" of hardness and toughness, calculated from a standard statistical ANOVA (ANalysis Of VAriables), are shown in Figures 4.9 and 4.10. The contribution of each component on hardness and toughness is given in Table 4.9. It appeared that the AlN addition was beneficial to the hardness, whereas, the TiO_2 was detrimental to the hardness. Composition also affected the toughness. The materials exhibiting high toughness had high amounts of TiO_2 and low amounts (or even none) of Al_2O_3. Combining both hardness and fracture toughness, it was clear that the optimum composition should have a high amount of AlN and a low amount of Al_2O_3. However, TiO_2 had different roles in hardness and toughness. With increasing the amount of TiO_2 additive, toughness increased, but hardness decreased. Therefore, an intermediate amount of TiO_2 (1%) appeared to be the best choice. In this study, Y_2O_3 did not affect either hardness or fracture toughness.

Table 4.9 Additive Contribution to Hardness and Toughness

	Contribution to Hardness	Contribution to Toughness
Y_2O_3	3 %	0 %
Al_2O_3	2 %	57 %
TiO_2	32 %	42 %
AlN	63 %	1 %
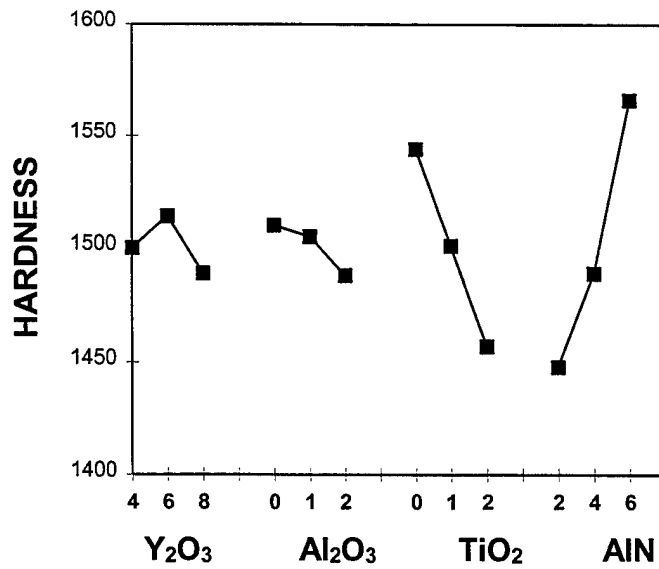
Figure 4.9 *Effect of Each Additive on the Response of Hardness (in kg/mm².)*
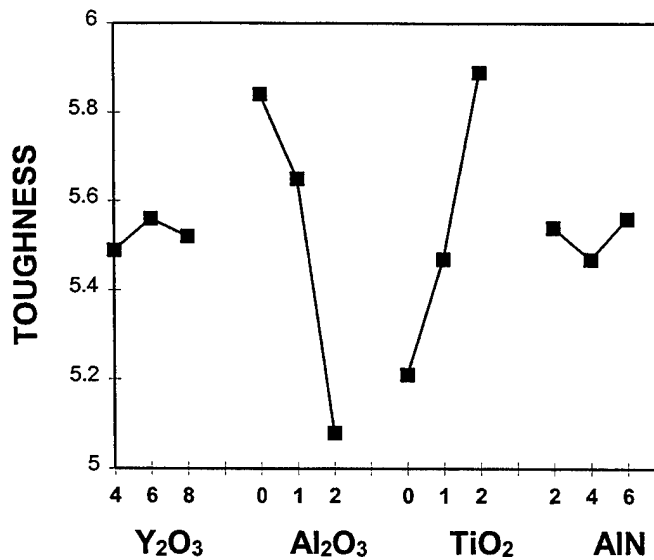
Figure 4.10 *Effect of Each Additive on the Response of Fracture Toughness (in MPa $\sqrt{m}$).*

4.2.2.1.5 Effect of the Addition of Ultra-fine Si_3N_4 Powder (Group F)

Microstructure always plays an important role in the mechanical behavior of a material. The objective of this set of compositions was to add some ultra-fine Si_3N_4

powders to produce a silicon nitride with small grain size. However, as shown in Figures 4.11 and 4.12, the addition of ultra-fine Si_3N_4 powder did not affect either hardness or toughness significantly.
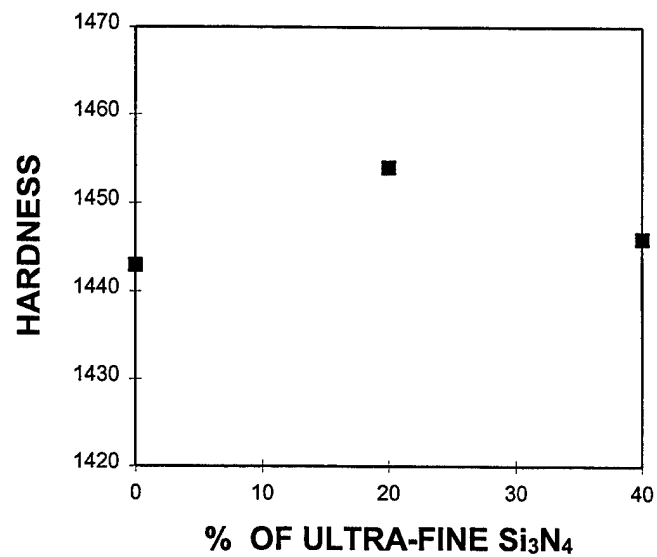
Figure 4.11 *Effect of the Addition of Ultra-fine Si_3N_4 Powder on Hardness (in kg/mm^2).*
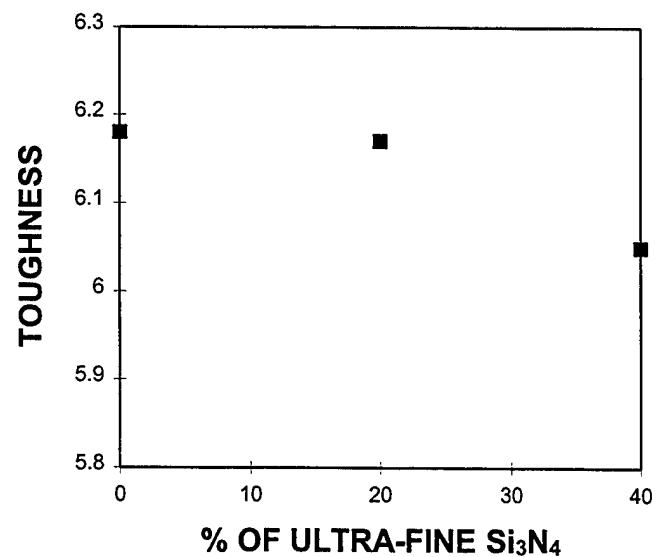
Figure 4.12 *Effect of the Addition of Ultra-fine Si_3N_4 Powder on Fracture Toughness (in MPa $\sqrt{m}$).*

4.2.2.1.6   Effect of Si Powder with Small Particle Size (Group G)

Fine microstructure should be achieved using small raw material. However, the results showed that small Si powder was not beneficial to either hardness or toughness, as shown in Figures 4.13 and 4.14.
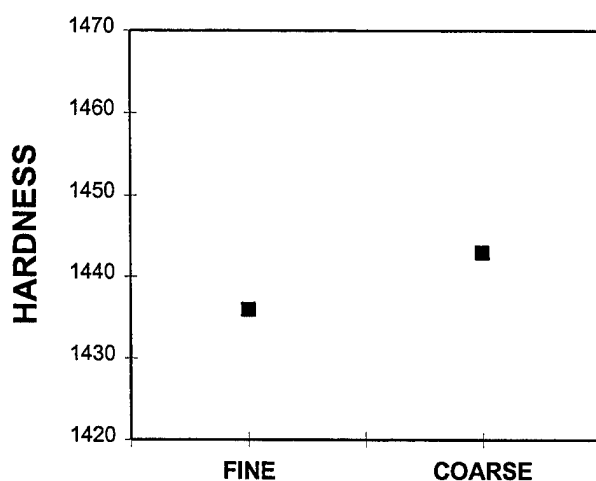
Figure 4.13   Effect of Silicon Particle Size on Hardness (in kg/mm²).
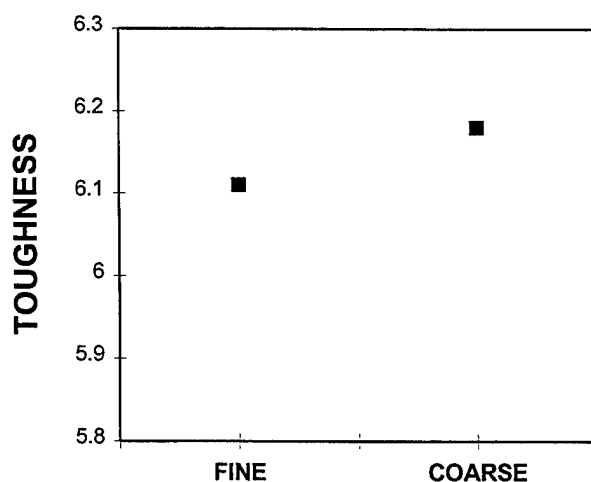
Figure 4.14   Effect of Silicon Particle Size on Fracture Toughness (in MPa √m).

4.2.2.2   Grain Size

The processing steps in the first iteration resulted in 100 different material samples representing 25 compositions and four sets of heat treating conditions (sintering + HIPing). The compositions and processing conditions are listed in Tables 4.3 and 4.6, respectively. The average grain sizes of specimens in sets 1, 3 and 4 were measured using SEM/BSE, and are shown in Table 4.10.

The grain size appeared to be influenced by the processing conditions. Materials processed under the lowest sintering and HIPing temperatures (condition No. 1) had the lowest average grain size (1.38 μm vs. 1.68 and 1.65 μm).

Grain size was also influenced by the compositions. Some qualitative assessments are summarized as follows:

1. Grain size decreased when the Al_2O_3/TiO_2 ratio increased.   (Group B)

2. Grain size decreased with increasing the Al_2O_3/AlN ratio.   (Group C)

3. Increasing the total amount of additives led to a decrease in grain size. (Group D)

4. The amount of TiO_2 had a dominant contribution over other additives. The greater the amount of TiO_2, the greater the grain size. (Group E)

5. The addition of 20% ultra-fine Si_3N_4 powder reduced the grain size slightly (from 1.49 μm to 1.36 μm). However, more addition of the ultra-fine powder did not change the average grain size. (Group F)

6. The use of small Si powder did not result in a reduced grain size. (Group G)

Table 4.10 – Grain Size of Specimens from the First Iteration

Group	No	Composition	Grain Size μm No. 1	No. 2	No. 3	Average Nos.1,3, 4
A	1	4/4/1/3	1.16	1.54	1.78	1.49
B	2	4/3/2/3	1.50	1.94	1.92	1.79
	3	4/2/3/3	1.56	1.88	2.00	1.81
	4	4/1/4/3	1.55	2.04	2.09	1.89
	5	4/0/5/3	1.76	2.75	2.22	2.24
C	6	4/3/1/4	1.28	1.70	1.68	1.55
	7	4/2/1/5	1.31	1.51	1.62	1.48
	8	4/1/1/6	1.38	1.61	1.61	1.53
	9	4/0/1/7	1.87	2.02	1.89	1.93
D	11	2/2/.5/1.5	1.54	1.72	1.67	1.64
	12	3/3/.75/2.25	1.35	1.65	1.62	1.54
	13	6/6/1.5/4.5	1.15	1.59	1.46	1.40
E	14	4/0/0/2	1.20	1.34	1.33	1.29
	15	4/1/1/4	1.13	1.51	1.43	1.36
	16	4/2/2/6	1.26	1.61	1.78	1.55
	17	6/0/1/6	1.46	1.29	1.50	1.42
	18	6/1/2/2	1.53	1.82	1.61	1.65
	19	6/2/0/4	1.32	1.50	1.47	1.43
	20	8/0/2/4	1.58	1.91	1.64	1.71
	21	8/1/0/6	1.30	1.40	1.64	1.45
	22	8/2/1/2	1.40	1.47	1.36	1.41
F	23	4/4/1/3/20	1.19	1.48	1.42	1.36
	24	4/4/1/3/40	1.21	1.45	1.37	1.34
G	25	4/4/1/3 Fine	1.23	1.55	1.54	1.44
	All	Average	1.38	1.68	1.65	
		Std. Dev.	0.16	0.22	0.18	

The correlations between hardness, fracture toughness and grain size were proposed by Mukhopadhyay[4] and Kawashima[5] as described in Section 2.2. Applying the same analogies and a linear regression method, the relationships between measured hardness, fracture toughness and the average grain size can be correlated as follows:

$$H = 1025 + 561 \ (G)^{-1/2} \quad kg/mm^2$$

$$K_{IC} = 2.05 + 2.90 \ (G)^{1/2} \quad MPa \ \sqrt{m}$$

where G is the grain size in μm. The coefficients in these two equations are different from the coefficients obtained in Mukhopadhyay's[4] and Kawashima's[5] programs, probably due to the different testing methods. Mukhopadhyay[5] measured the Vickers hardness using 10 kg of loading; whereas we used 5 kg. Kawashima[5] measured fracture toughness using a Japanese Single-Edge-Precracked-Beam (SEPB) method, and we used an indentation technique.

Hardness, fracture toughness and the correlation equations are shown in Figures 4.15 and 4.16. Overall, hardness decreased and fracture toughness increased with increasing grain size. However, the scattering of data (especially for the fracture toughness) suggested grain size was not the only determining factor for the properties. As shown in the correlation equations, the grain size should be smaller than 1.1 μm to have hardness higher than 1550 kg/mm² and should be larger than 1.9 μm to exhibit fracture toughness higher than 6.0 MPa $\sqrt{m}$. However, our results showed that the 6/0/1/6 material, having a grain size in the range between 1.3 and 1.5 μm, can meet the Class I hardness and fracture toughness requirements. Other microstructure features must be contributing to the hardness and fracture toughness.
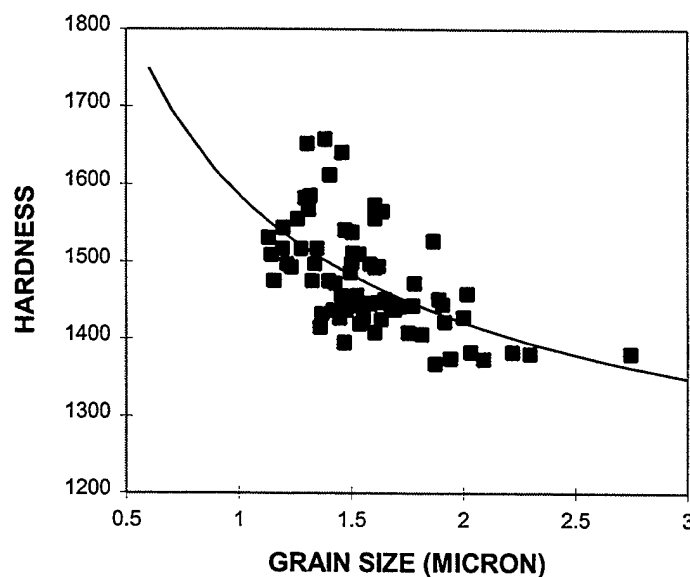
Figure 4.15   Relationship Between Hardness (in kg/mm²) and Grain Size.

50
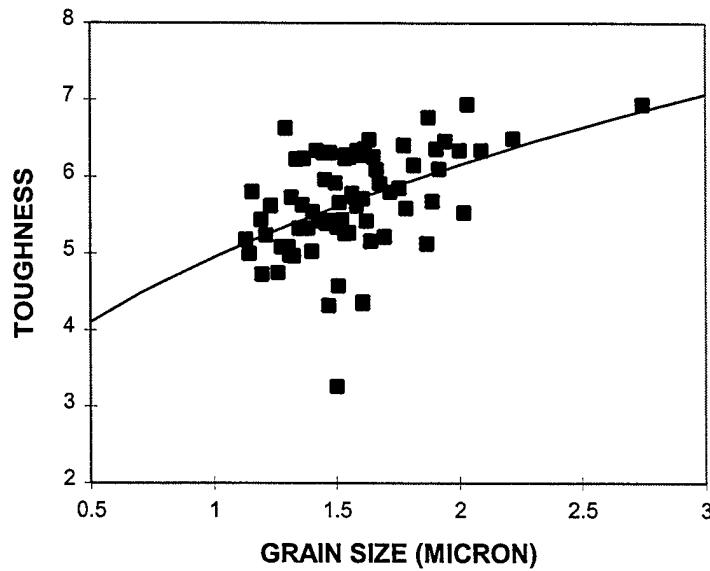
Figure 4.16 *Relationship Between Fracture Toughness (in MPa $\sqrt{m}$) and Grain Size.*

4.2.2.3 Microstructure

The processing steps in the first iteration resulted in 100 different material samples representing 25 compositions and four sets of heat treating conditions (sintering + HIPing). The compositions and processing conditions are listed in Tables 4.3 and 4.6, respectively. Specimens from processing condition No. 1 and 3 were characterized using x-ray diffraction (XRD). The types of intergranular phases and α-Si_3N_4 content are listed in Table 4.11. To understand the microstructure development during processing, a set of sintered specimens was also characterized, as listed in Table 4.11. This set of specimens was sintered at 1700°C, representing the materials before HIPing, for the processing conditions Nos. 1, 2 and 4. The XRD results from the nitrided materials (prior to sintering) are also listed in the same table.

4.2.2.3.1 Effect of Intergranular Phases

Hardness and fracture toughness are correlated to the type of intergranular phase, as shown in Figures 4.17 and 4.18. The open squares represent the materials processed at low temperatures (condition No. 1, 1700°C sintering and 1875°C HIPing)

51

whereas the solid diamonds are the materials processed at high temperatures (condition No. 3, 1750°C sintering and 1950°C HIPing). It appeared that the materials processed at lower temperatures (open squares) had slightly higher hardness and lower fracture toughness than the materials processed at high temperatures (solid diamonds). Results also indicated that the silicon nitride with a crystalline intergranular phase had a higher hardness than the material with an amorphous intergranular phase. The scattering in the data may be attributed to the differences in the total amounts and compositions of the intergranular phases. Nevertheless, the type of intergranular phase did not affect the fracture toughness.

Table 4.11   Summary of XRD Results for the First Iteration

	No.	Composition	Sinter-HIP No.1		Sinter-HIP No. 3		Sinter Only 1700°C		Nitrided (RBSN)
			Inter-granular	$\alpha/(\alpha+\beta)$ %	Inter-granular	$\alpha/(\alpha+\beta)$ %	Inter-granular	$\alpha/(\alpha+\beta)$ %	$\alpha/(\alpha+\beta)$ %
A	1	4/4/1/3	A	0	A	0	A	0	25
B	2	4/3/2/3	A	0	A	0	A	0	35
	3	4/2/3/3	A	0	A	0	A	0	30
	4	4/1/4/3	A	0	A	0	A	0	28
	5	4/0/5/3	A	0	A	0	A	0	27
C	6	4/3/1/4	C	0	A	0	C	0	38
	7	4/2/1/5	C	17	C	15	C	12	48
	8	4/1/1/6	C	23	C	32	C	22	42
	9	4/0/1/7	C	7	A	0	C	9	64
D	11	2/2/.5/1.5	C	0	A	0	C	0	50
	12	3/3/.75/2.25	A	0	A	0	A	0	40
	13	6/6/1.5/4.5	A	0	N/A	N/A	C	0	30
E	14	4/0/0/2	C	0	C	0	C	0	55
	15	4/1/1/4	C	0	C	0	C	0	54
	16	4/2/2/6	C	10	A	8	C	9	49
	17	6/0/1/6	C	35	C	36	C	32	42
	18	6/1/2/2	A	0	A	0	C	0	41
	19	6/2/0/4	C	16	C	16	C	11	53
	20	8/0/2/4	C	0	C	0	C	0	48
	21	8/1/0/6	C	40	C	40	C	36	65
	22	8/2/1/2	C	0	C	0	C	0	41
F	23	4/4/1/3/20	A	0	A	0	A	0	23
	24	4/4/1/3/40	A	0	A	0	C	0	20
G	25	4/4/1/3 Fine	A	0	A	0	A	0	34

A: Amorphous Intergranular Phase
C: Crystalline Intergranular Phase
N/A: not Analyzed
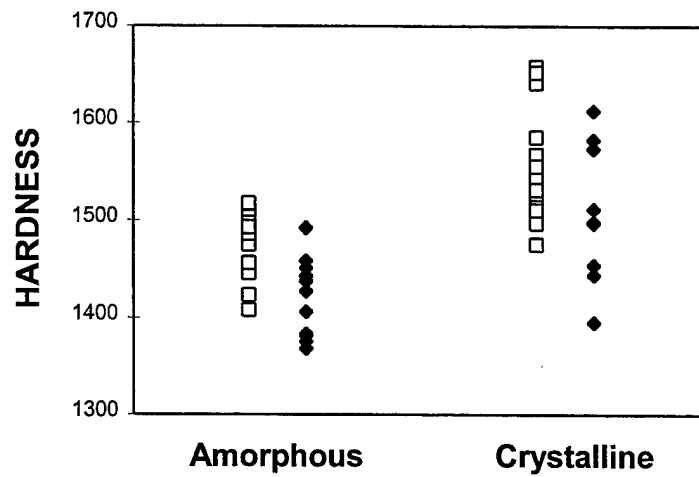
Figure 4.17   *Relationship Between Hardness (in kg/mm²) and Types of Intergranular Phase.*
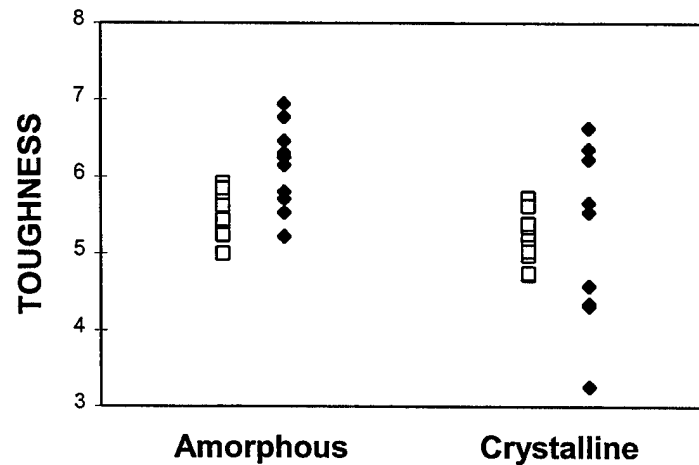
Figure 4.18   *Relationship Between Fracture Toughness (in MPa √m̄) and Types of Intergranular Phase.*

4.2.2.3.2   Effect of α- and β-Si₃N₄

As shown in Table 4.11, several compositions have substantial amounts of preserved α-Si₃N₄ in their final densified forms. Hardness and fracture toughness are correlated to the α contents in Figures 4.19 and 4.20. The open squares represent the materials processed at low temperatures (condition No. 1, 1700°C sintering and 1875°C

HIPing); whereas the solid diamonds are the materials processed at high temperatures (condition No. 3, 1750°C sintering and 1950°C HIPing). Remarkably, both sets of specimens show a linear relationship between hardness and the α-Si_3N_4 content. A linear regression technique was applied to these data, and results are:

$$H = 1490 + 4.74 (\alpha\%) \quad kg/mm^2 \quad \text{Condition No. 1 (Low Temp)}$$

$$H = 1427 + 4.61 (\alpha\%) \quad kg/mm^2 \quad \text{Condition No. 3 (High Temp)}$$

where $\alpha\%$ is the percentage of α-Si_3N_4. Both sets of data apparently have the same relationship between hardness and the α-Si_3N_4 content. The difference in the slopes is merely 2%, so that these two lines are almost parallel. The difference in the intercepts in these two linear equations, which is attributable to the difference in grain size, is only 5%. As shown in Table 4.10, the average grain size of all specimens from condition No. 1 (low temperature process) is 1.38 μm, whereas, the average grain size of all specimens from condition No. 3 (high temperature process) is 1.65 μm. This 20% difference in grain size leads to a 5% difference in the intercepts and a 5% difference in the average hardness (see Table 4.8). Meanwhile, a 10% increase in hardness can be expected if the silicon nitride has a 30% increase in the α-Si_3N_4 content. Results indicate that the hardness of a silicon nitride body is determined by both the α-Si_3N_4 content and grain size.

However, the relationship between fracture toughness and the α-Si_3N_4 content is not obvious. α-Si_3N_4 usually has a lower fracture toughness than β-Si_3N_4, but the materials containing high amounts of hard α-Si_3N_4 do not necessarily have low fracture toughness. We concluded that fracture toughness is mainly related to the aspect ratio and fraction of acicular β-Si_3N_4 grains, instead of the total amount of β-Si_3N_4. The β-Si_3N_4 occurs as a mixture of acicular and equiaxed grains. Increasing the content of acicular β-Si_3N_4 increases the fracture toughness.
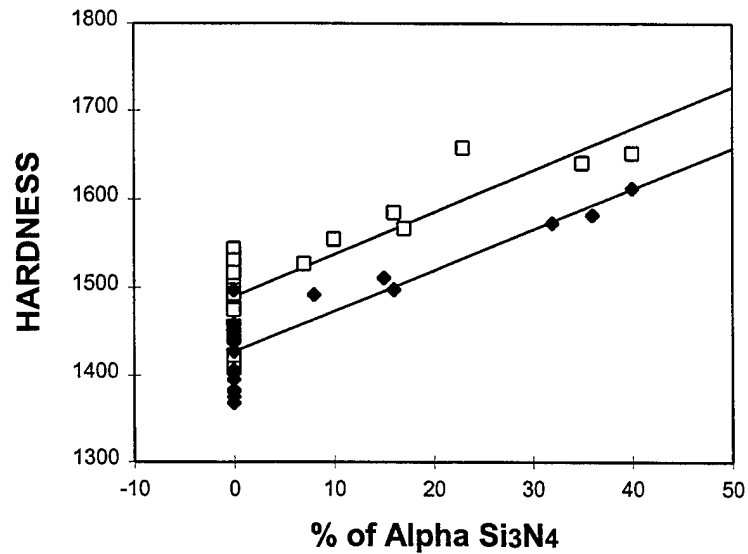
Figure 4.19 *Hardness (in kg/mm²) of Different Compositions Plotted as a Function of Their Alpha Phase Content.*
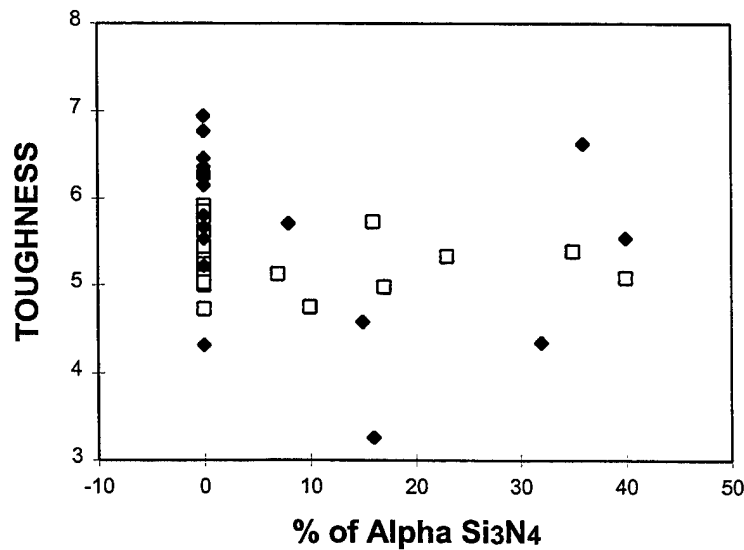
Figure 4.20 *Fracture Toughness (in MPa√m) of Different Compositions Plotted as a Function of Their Alpha Phase Content.*

The acicular grain growth of β-Si_3N_4 is a diffusion controlled reaction. During sintering and HIPing, the previously dissolved atoms diffuse through the liquid phase and precipitate onto the surface of existing β-Si_3N_4 nuclei[7]. Therefore, the acicular grain growth of β-Si_3N_4 can be promoted through the use of nucleation agents and high temperature heat treatment. The heat treatment can be incorporated into either the

sintering or HIPing step. Hoffman et.al. have demonstrated the efficacy of β-Si_3N_4 powder as a nucleation agent[8]. During our original program, we observed an effect of TiO_2 addition on the promotion of acicular grain growth, as described in Section 2.1. We believed that TiO_2 (or its resultant TiN) can serve as a nucleation agent to promote the acicular grain growth and to improve the fracture toughness.

α-Si_3N_4 is usually considered to be a low temperature phase. At high temperatures, α-Si_3N_4 transforms to β-Si_3N_4 through a dissolution-precipitation process. However, certain atoms, such as Y and Yb, can occupy the large interstitial sites inside the α-Si_3N_4 lattice and stabilize the α-Si_3N_4 phase. Y_2O_3 is one of our sintering additives and Y serves as the stabilizing atom. Since Y has a much higher atomic number than Si and N, the stabilized α-Si_3N_4 would have a higher average atomic number than the β-Si_3N_4; as a result, the stabilized α-Si_3N_4 grains appear brighter than the β-Si_3N_4 grains in an SEM image. Therefore, a "partially stabilized" silicon nitride exhibits a mixture of a bright intergranular phase, a light-gray stabilized α-Si_3N_4 and a dark-gray β-Si_3N_4 phase. "Partially stabilized" silicon nitride refers to a material containing a mixture of α- and β-Si_3N_4. To achieve both high hardness and high fracture toughness simultaneously, not all of the α-Si_3N_4 should be stabilized. Contrarily, a "non stabilized" silicon nitride (no α-Si_3N_4) does not have the light gray α-Si_3N_4 grains in the SEM micrograph.

Selective SEM micrographs and properties of a partially stabilized (6/0/1/6) and a non stabilized (4/1/1/4) silicon nitride are shown in Figure 4.21. The 3000X micrographs clearly show the light-gray stabilized α-Si_3N_4 phase, and the 1000X micrographs are appropriate to qualitatively examine the aspect ratio of acicular β-Si_3N_4 grains. The two materials in Figure 4.21 were processed through the same condition (Set No. 3), having a slight difference in composition, but they exhibited a dramatic difference in microstructure and properties.
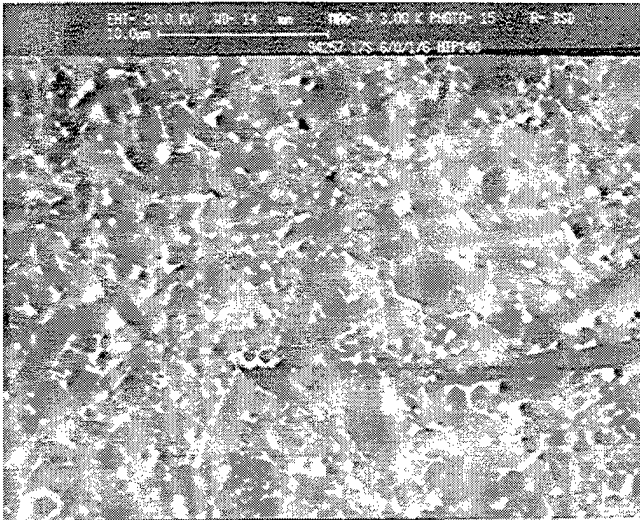
3000X   3000X
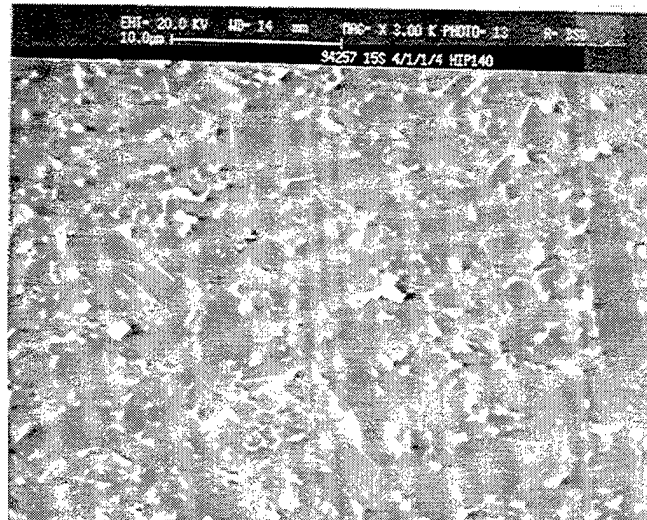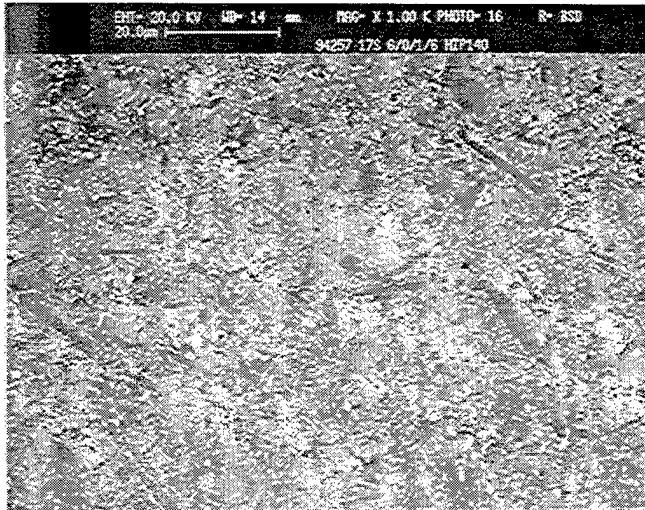
1000X   1000X
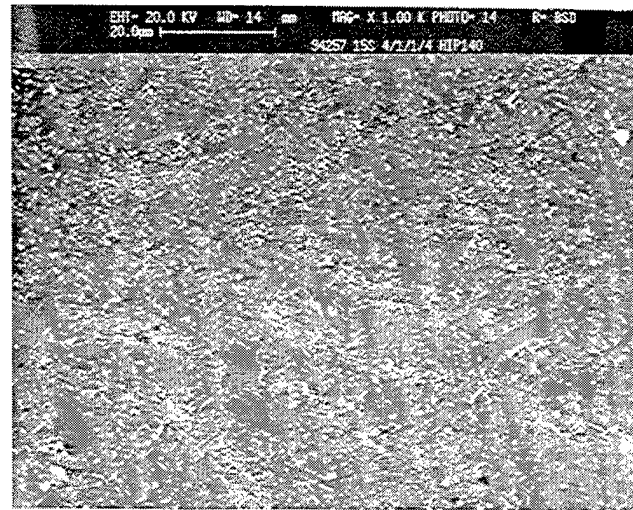
Partially Stabilized Silicon Nitride		Non-Stabilized Silicon Nitride	
Composition	6/0/1/6	Composition	4/1/1/4
$\alpha/(\alpha+\beta)$ %	36	$\alpha/(\alpha+\beta)$ %	0
Hardness kg/mm^2	1582	Hardness kg/mm^2	1454
Toughness MPa$\sqrt{m}$	6.63	Toughness MPa$\sqrt{m}$	5.66
Intergranular Phase	Crystalline	Intergranular Phase	Crystalline
Grain Size μm	1.50	Grain Size μm	1.43

Figure 4.21   *Micrographs and Properties of Partially Stabilized and Non-stabilized Silicon Nitride*

The partially stabilized material (6/0/1/6) had a substantial amount of α-Si_3N_4 (36%), resulting in high hardness (1582 kg/mm^2). In contrast, the non stabilized silicon nitride (4/1/1/4) did not contain α-Si_3N_4 and exhibited low hardness (1454 kg/mm^2). The partially stabilized silicon nitride, containing less β-Si_3N_4 phase than its non stabilized counterpart, does not necessarily have a low fracture toughness. The aspect ratio of acicular β-Si_3N_4 grains and the chemistry of the grain boundary determine the efficacy of the toughening mechanisms. As shown in Figure 4.21, the partially stabilized silicon nitride (6/0/1/6) appears to have more and longer acicular grains than the non stabilized material (4/1/1/4). As a result, the partially stabilized silicon nitride (6/0/1/6) has both high hardness and fracture toughness.

4.2.3   Microstructure Development of Partially Stabilized Silicon Nitride

A partially stabilized silicon nitride containing optimal amounts of "hard" α-Si_3N_4 and "tough" acicular β-Si_3N_4 grains with high aspect ratio will have outstanding hardness and fracture toughness. The microstructure development and its associated additive compositions and processing parameters are discussed in this section.

As shown in Table 4.11, only the materials containing 4% or more AlN have the stabilized α-Si_3N_4. For example, in the composition Group C, the amount of stabilized α-Si_3N_4 increases with increasing AlN addition, except for the material without Al_2O_3 (the 4/0/1/7 composition). This is shown in Figure 4.22, where open squares represent the low temperature process (condition No. 1) and solid diamonds represent the high temperature process (condition No. 3). The 4/0/1/7 composition contains 7% of AlN, but retains only a moderate amount of stabilized α-Si_3N_4 (7% from condition No. 1 and 0% from condition No. 3). Apparently, there are some interactions between additives. Since the composition (4/0/1/7) does not follow the trend for the stabilized α-Si_3N_4 development, it is not surprising that its hardness and fracture toughness deviate from the trends for the same composition group (Section 4.2.2.1.2).

The α-Si_3N_4 content was correlated to each additive, using the composition Group E (a factorial experimental matrix). The contribution of each additive is given in

Table 4.12, and the response for stabilized α-Si$_3$N$_4$ is shown in Figure 4.23. To have a high amount of stabilized α-Si$_3$N$_4$, the material should have a high amount of AlN (6%), a high amount of Y$_2$O$_3$ (6-8%), a low amount of Al$_2$O$_3$ (0-1%) and a low amount of TiO$_2$ (0-1%).

Table 4.12   Contribution of Additives to Stabilized α-Si$_3$N$_4$

Additive	Contribution
Y$_2$O$_3$	16 %
Al$_2$O$_3$	2 %
TiO$_2$	18 %
AlN	64 %
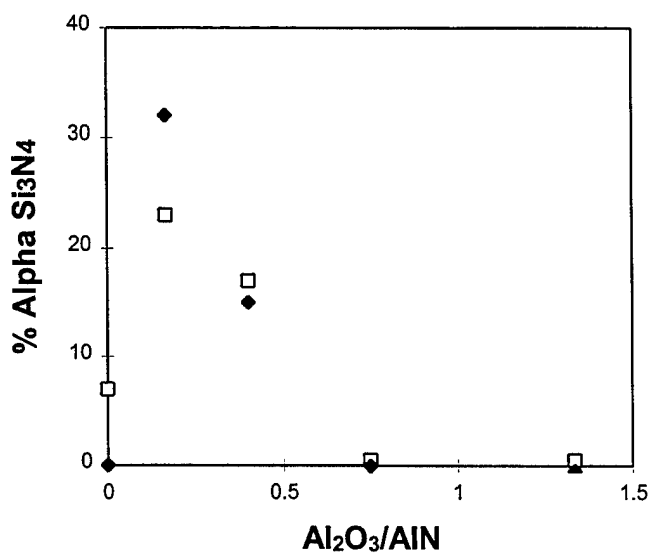
Figure 4.22   *Relationship Between α-Si$_3$N$_4$ Content and the Al$_2$O$_3$/AlN Ratio.*
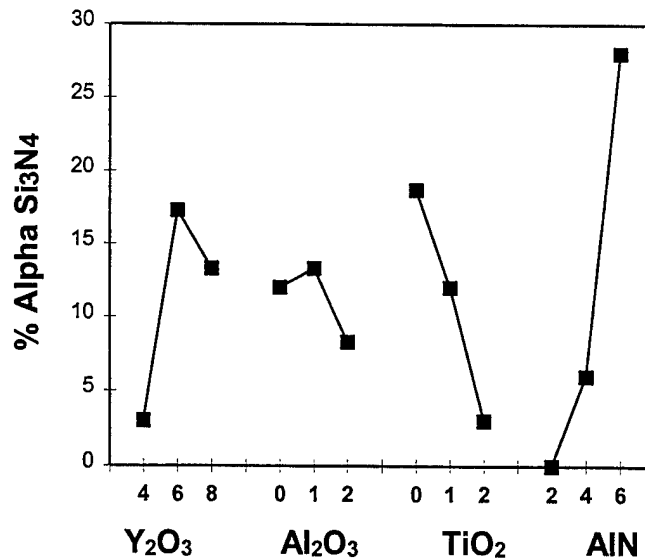
Figure 4.23   *A Summary Chart Showing the Effect of Additives on Stabilized α Si_3N_4.*

A set of sintered specimens and a set of nitrided specimens were characterized using XRD to study the microstructure development. The relationship of stabilized α-Si_3N_4 before and after a 1875°C HIPing was examined by comparing the α-Si_3N_4 content after sintering and after HIPing, as shown in Figure 4.24. Results indicate that there is no change in α-Si_3N_4 content during HIPing, since the α-Si_3N_4 content before HIPing is identical to the one after HIPing. The high thermal stability of α-Si_3N_4 allows us to HIP the materials at very high temperatures to promote the acicular β-Si_3N_4 grains for high toughness, without a loss in hard α-Si_3N_4. Although the high temperature HIPing may induce grain growth and may result in a decrease in hardness, a sufficient amount of hard α-Si_3N_4 can still make the material meet the Class I hardness requirement.

However, there is no one-to-one correlation in α content before and after sintering, as shown in Figure 4.25. High amounts of α-Si_3N_4 before sintering do not guarantee high amounts of α-Si_3N_4 after sintering. Nonetheless, if the nitrided part does not have any α-Si_3N_4 phase, it will not have any stabilized α-Si_3N_4 after sintering. The α-Si_3N_4 content in a nitrided part is determined by the additive composition, as

described in Section 4.2.1. Therefore, we concluded that the amount of stabilized α-Si_3N_4 would be partially determined by the additive composition.

Comparing the α-Si_3N_4 during each processing stage, we concluded that the α stabilization process occurred mainly during sintering. Once the α-Si_3N_4 was stabilized, it would not transform to β-Si_3N_4.
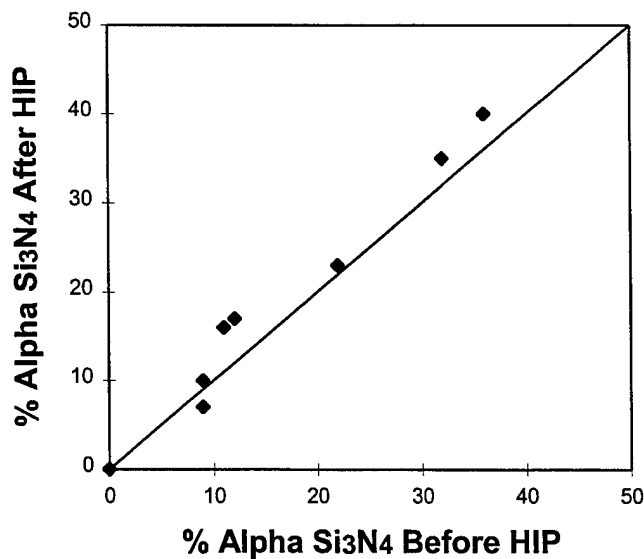
Figure 4.24   *Relationship of α-Si_3N_4 Before and After 1875°C HIPing.*
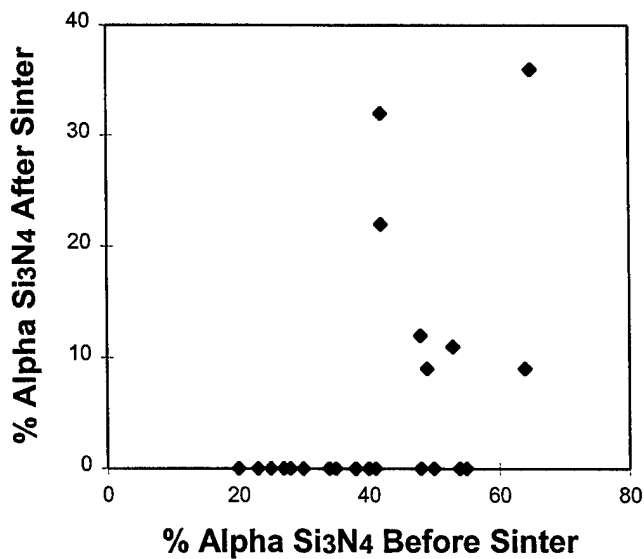
Figure 4.25   *Relationship of α-Si_3N_4 Before and After 1700°C Sintering.*

61

During sintering, the diffusion controlled α stabilization process competes with the $\alpha \rightarrow \beta$ transformation process, and both processes are governed by temperatures and compositions. High sintering temperatures can not only accelerate the stabilization process, to retain α-Si_3N_4, but also promote the $\alpha \rightarrow \beta$ transformation, leading to a loss of α-Si_3N_4. The result of the competing reactions can be visualized in Figure 4.26. To achieve a maximum amount of α-Si_3N_4, the temperature must be at its optimum.
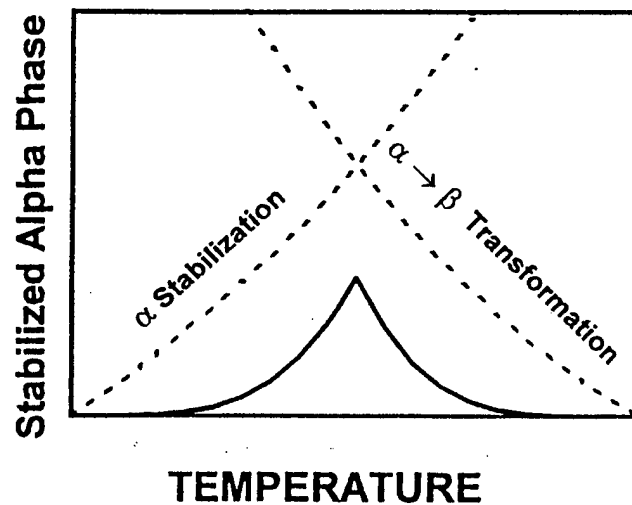
Figure 4.26   *Competition Between Stabilization and Transformation.*

4.2.4 Summary of the First Iteration

One hundred specimens, representing 25 compositions and four processing conditions, were fabricated and characterized during the first iteration. We demonstrated that hardness and fracture toughness can be improved simultaneously through microstructure optimization. A silicon nitride containing optimized amounts of "hard" α-Si_3N_4 and "tough" acicular β-Si_3N_4 can have both high hardness and fracture toughness. Grain size can also affect both hardness and fracture toughness, and the grain size is determined by the additive composition and processing temperatures. The α stabilization, $\alpha \rightarrow \beta$ transformation, and β-Si_3N_4 acicular grain growth processes are

carried out through a liquid phase and can be tailored through a composition and process design.

4.3 Selection of Promising Compositions (Second Iteration)

The objective of the second iteration was to re-evaluate and to confirm the results from the first iteration. As described in Section 4.2.2.1, the 6/0/1/6 composition could meet the Class I requirements while using high temperature HIPing. This composition served as a reference for selecting a new set of compositions, as listed in Table 4.13. Because 6/0/1/6 was the most promising composition, two powder batches were prepared in this iteration.

Table 4.13   Additive Composition for the Second Iteration

Group	No.	Composition $Y_2O_3/Al_2O_3/TiO_2/AlN$ in wt%
A	26	6/0/1/6
	27	7/0/1/5
	28	8/0/1/4
(B)	29	8/0/1/6
B	30	6/0/0/4
	31	6/0/1/6
	32	6/1/1/6
	33	6/1/0/4
	34	8/0/0/4
	35	8/1/1/6
	36	8/1/1/4
C	37	4/4/1/3

Based on the selection rationales, these compositions can be divided into three groups. Composition No. 29 (8/0/1/6) was used for both groups A and B.

A. Vary the ratio of AlN/Y_2O_3, holding all else constant. In the first iteration, we observed a significant influence of AlN on both hardness and fracture toughness. This set of experiments was designed to confirm the result.

B. Expand the composition range using a partial factorial array based on a two-level factorial test plan, as described in Table 4.14. The experimental matrix used the most promising composition (6/0/1/6) as a reference. The amount of

63

each additive was selected so that maximum hardness and fracture toughness could be expected.

C. Use composition (4/4/1/3) as a baseline, a composition developed in the original program. This composition was also included in the first iteration.

Table 4.14   Two-Level Factorial Test Plan in the Second Iteration

Factor	Level 1	Level 2
Y_2O_3	6 %	8 %
Al_2O_3	0 %	1 %
TiO_2	0 %	1 %
AlN	4 %	6 %

Since the processing conditions are important for creating the proper properties, four processing conditions were used in this iteration, as listed in Table 4.15. The sintering time and HIPing time were 10 hours and 75 minutes, respectively. However, not all of the compositions reached full density using some of the four processing conditions, as shown in Table 4.16. It appeared that the materials having no "oxygen pumps" (Al_2O_3 and TiO_2), e.g. 6/0/0/4 and 8/0/0/4, were difficult to densify. Nonetheless, while using high processing temperatures (condition No. 4), these compositions can still reach their full density. The results demonstrated the close relationship between compositions and required processing temperatures for densification.

Table 4.15   Processing Conditions for the Second Iteration

Condition	Sintering Temperature °C	HIPing Temperature °C
1	1700	1850
2	1700	1900
3	1700	1950
4	1750	1950

Table 4.16   Density of Specimens from the Second Iteration

		Condition No.	1	2	3	4
		Sintering Temp	1700°C	1700°C	1700°C	1750°C
		HIPing Temp	1850°C	1900°C	1950°C	1950°C
Group	No.	Composition	Density g/cm³	Density g/cm³	Density g/cm³	Density g/cm³
A	26	6/0/1/6	3.27	3.27	3.26	3.27
	27	7/0/1/5	3.28	3.28	3.27	3.28
	28	8/0/1/4	3.29	3.30	3.29	3.29
(B)	29	8/0/1/6	3.29	3.30	3.28	3.30
B	30	6/0/0/4	2.94	2.79	3.01	3.26
	31	6/0/1/6	3.26	3.27	3.25	3.27
	32	6/1/1/6	3.26	3.26	3.25	3.26
	33	6/1/0/4	3.26	3.26	3.26	3.26
	34	8/0/0/4	2.90	2.84	2.97	3.29
	35	8/1/1/6	3.20	3.28	3.27	3.28
	36	8/1/1/4	3.29	3.30	3.29	3.30
C	37	4/4/1/3	3.23	3.23	3.23	3.23

Hardness and fracture toughness were measured only on fully dense materials, as listed in Table 4.17. Results showed that both 6/0/1/6 and 8/0/1/6 compositions can reach Class I requirements, when processed at high temperatures. The 7/0/1/5, 8/0/1/4, 8/0/1/6 and 8/1/1/4 compositions were very promising, as shown in the shaded areas in Table 4.17.

Both batch Nos. 26 and 31 had the same composition (6/0/1/6); however, it appeared that materials from batch No. 26 always had slightly higher fracture toughness than the materials from batch No. 31. It was suspected that there was a slight variation in powder composition. In order to preclude the lot-to-lot variation in fabricating program deliverables, all powders should be cross-blended to produce one large single homogeneous powder lot.

Table 4.17   Hardness and Fracture Toughness of Specimens from the Second Iteration

(H = Hardness in kg/mm^2; K$_{IC}$ = Fracture Toughness in MPa $\sqrt{m}$)

		Condition	1		2		3		4	
		Sintering Temp	1700°C		1700°C		1700°C		1750°C	
		HIPing Temp	1850°C		1900°C		1950°C		1950°C	
Group	No.	Composition	H	K$_{IC}$	H	K$_{IC}$	H	K$_{IC}$	H	K$_{IC}$
A	26	6/0/1/6	1581	5.98	1612	6.00	1575	5.74	1554	6.26
	27	7/0/1/5	1535	5.92	1551	5.63	1464	4.80	1500	6.36
	28	8/0/1/4	1492	5.90	1524	6.31	1462	3.99	1482	6.52
(B)	29	8/0/1/6	1562	5.62	1593	5.79	1560	5.44	1561	6.41
B	30	6/0/0/4							1520	5.02
	31	6/0/1/6	1557	5.55	1589	5.68	1580	5.43	1577	5.82
	32	6/1/1/6	1635	4.72	1592	4.94	1573	3.42	1617	4.67
	33	6/1/0/4	1545	5.46	1490	5.10	1463	5.58	1473	6.03
	34	8/0/0/4							1543	5.23
	35	8/1/1/6			1626	4.70	1531	3.85	1648	4.85
	36	8/1/1/4	1536	6.11	1498	6.22	1462	5.26	1510	6.56
C	37	4/4/1/3	1504	5.16	1447	6.00	1479	6.06	1464	6.13

Correlation between properties and compositions was determined. Since there were a few compositions not reaching full density, a complete analysis on Group B could not be carried out.

4.3.1 Effect of the Ratio of AlN to Y$_2$O$_3$

The relationship between hardness, fracture toughness and the AlN/Y$_2$O$_3$ ratio is shown in Figures 4.27 and 4.28. It appeared that both hardness and fracture toughness increased as the AlN/Y$_2$O$_3$ ratio increased. The most promising composition (6/0/1/6) appeared to be the most suitable one, according to this set of experiments.
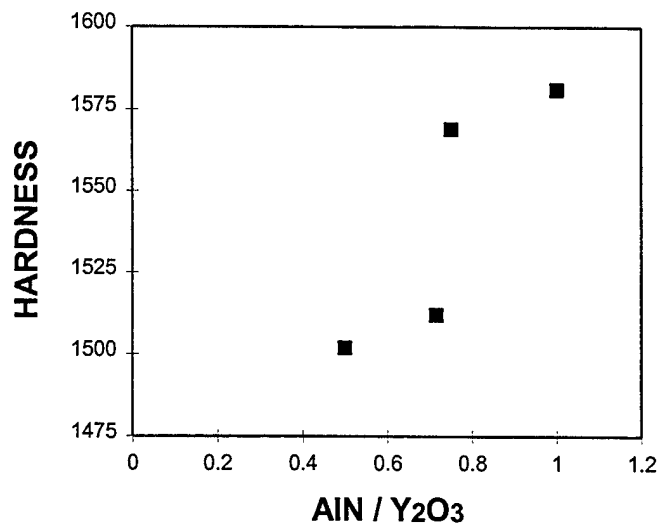
Figure 4.27   *Effect of the AlN to Y_2O_3 Ratio on Hardness (in kg/mm^2).*
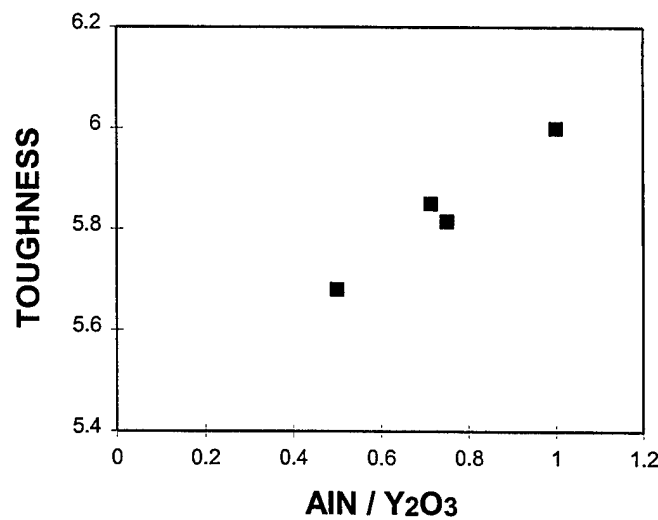
Figure 4.28   *Effect of the AlN to Y_2O_3 Ratio on Fracture Toughness (in MPa $\sqrt{m}$).*

4.3.2 Analysis of the Partial Factorial Design of Experiment for the Second Iteration

Because some of the compositions did not reach full density, a complete ANOVA for all conditions could not be performed. Only the materials processed in condition No. 4 were evaluated for the partial design of experiment. The calculated responses of

hardness and fracture toughness are shown in Figures 4.29 and 4.30. Results showed that the best material should have a high amount of AlN because of its influence on hardness. TiO_2 addition reduced the hardness; however, it had a significant contribution to fracture toughness. Y_2O_3 and Al_2O_3 did not appear to have much influence on either hardness or fracture toughness. The best composition from this ANOVA appeared to be 8/0/1/6; nevertheless, 6/0/1/6 had similar hardness and fracture toughness. Since the 6/0/1/6 composition was processed and characterized in both iterations, its microstructure development was relatively well known. Therefore, 6/0/1/6 was selected as the final composition.
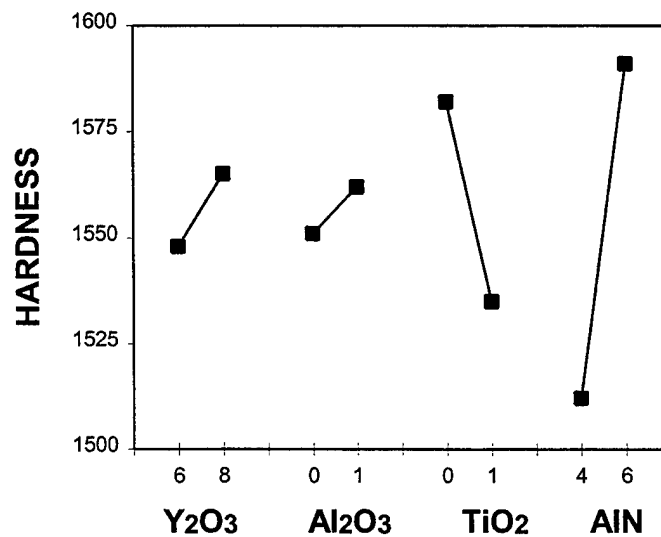

Figure 4.29 *Effect of Each Additive on the Response of Hardness (in kg/mm²) for Specimens from Condition No. 4 in the Second Iteration.*
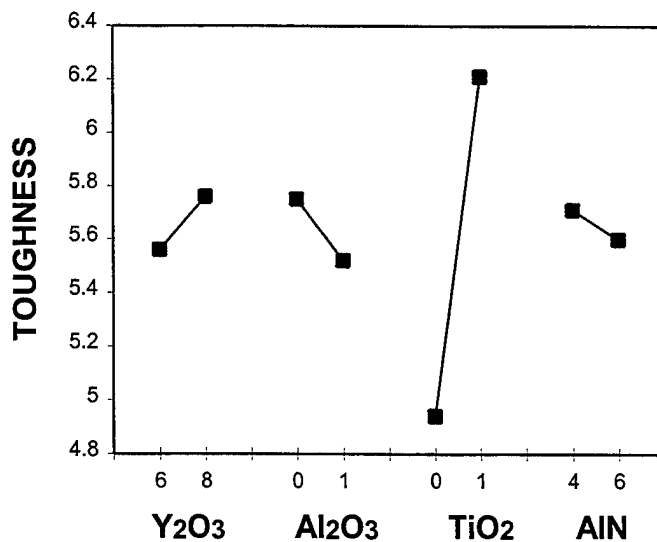
Figure 4.30 *Effect of Each Additive on the Response of Fracture Toughness (in MPa $\sqrt{m}$) for Specimens from Condition No. 4 in the Second Iteration.*

4.3.3 Variation in Microstructure and Properties of the Down-selected Composition

The second iteration confirmed the results from the first iteration: silicon nitride can achieve high hardness and fracture toughness through a composition and process parameter design. The final composition was selected as 6/0/1/6. However, some variations in hardness and fracture toughness were noted. A few selected 6/0/1/6 materials in this iteration were characterized using XRD. Results are listed in Table 4.18. Some observations were made in this microstructure/property comparison:

- There was a lot-to-lot variation both in powder batching and temperature control.

- Hardness and fracture toughness were sensitive to the microstructure. Subtle variations in processing may cause a difference in microstructure and properties.

- Overall, the variation in microstructure features and properties was within the range of 5 to 10%.

69

Table 4.18 Microstructure Features and Properties of the 6/0/1/6 Composition from Different Powder Batches and Different Processing Conditions

No.	Sintering Temperature °C	HIPing Temperature °C	$\alpha/(\alpha+\beta)$	Grain Size μm	Hardness kg/mm^2	Toughness MPa $\sqrt{m}$	Class
17	1700	1875	35%	1.46	1641	5.39	II
17	1750	1950	36%	1.50	1582	6.63	I
26	1700	1950	30%	1.46	1575	5.74	II
26	1750	1950	36%	1.64	1554	6.26	I
31	1750	1950	30%	1.42	1577	5.82	II

4.4 Process Optimization

The two composition/processing parameter iterations evaluated a total of 31 different compositions. The final composition has been down-selected as 6/0/1/6 (6% Y_2O_3, 1% TiO_2 and 6% AlN). During this program, we learned that silicon nitride exhibiting superior hardness and toughness can be fabricated through a form of microstructural control. The material must contain both "hard" α-Si_3N_4 and "tough" acicular β-Si_3N_4 phases. HIPing temperatures as high as 1950°C were used in these two composition iteration studies to promote the acicular grain growth of β-Si_3N_4, and to enhance the fracture toughness. However, our recent experience in ball-valve fabrication indicated that this temperature was not appropriate for ball blank manufacturing. At temperatures higher than 1850°C, balls tend to bond together and form some "necking". As a result, chips on ball surfaces occurred when individual balls were separated during unloading. These chips significantly reduced the manufacturing yield. To successfully transfer the R&D effort to bearing manufacturing, processing conditions must be optimized. The process optimization emphasized the promotion of acicular β-Si_3N_4 grain growth during sintering. The sintering step must develop not only optimized amounts of "hard" α-Si_3N_4 phase, but also optimized amounts of "tough" acicular β-Si_3N_4 phase. The subsequent HIPing operation, therefore, needs only to remove the residual porosity. As a result, the HIPing temperatures can be reduced to below 1850°C, which would be more suitable for bearing manufacturing.

Three sets of experiments were conducted to optimize the processing parameters for the 6/0/1/6 composition. The experiments included a set of isothermal sintering experiments and two two-level factorial experimental matrices. After sintering, all specimens were HIPed at 1825°C for 75 minutes. All HIPed test specimens had the same density, 3.27 g/cm³. Metallographic examination showed no evidence of porosity. Hardness and toughness were measured for all specimens. Results were encouraging, and indicated that the optimized sintering conditions can fabricate a Class I bearing material without using a high temperature HIPing.

4.4.1 Isothermal Sintering

Three sintering runs, with different sintering times, were performed at the same temperature (1750°C) to evaluate the kinetics of microstructure development. Hardness and toughness are listed in Table 4.19. The results showed that long sintering reduced the hardness, but enhanced the fracture toughness, probably due to the grain size effect.

Table 4.19 Hardness and Fracture Toughness of Specimens from the Isothermal Sintering Experiments in the Process Optimization

Sintering Time	Hardness kg/mm²	Toughness MPa $\sqrt{m}$	Class
6 Hrs	1575	5.89	II
10 Hrs	1561	6.22	I
14 Hrs	1540	6.52	II

4.4.2 The First Two-level Factorial Design of Experiment for Process Optimization

The first DOE evaluated the effect of sintering temperature, time and atmosphere, using the Taguchi technique. Hardness and fracture toughness are listed in Table 4.20. ANOVA indicated a strong influence of sintering time on hardness and a significant influence of sintering temperature and time on fracture toughness. Sintering

71

atmosphere did not affect either hardness or fracture toughness. The contributions of these sintering parameters are listed in Table 4.21. To achieve both high hardness and fracture toughness, the best choice appeared to be using high temperature (1775°C) and short sintering time (6 Hrs).

Table 4.20. Hardness and Fracture Toughness of Specimens
from the First Factorial DOE in the Process Optimization

Sintering Temp	Sintering Time	Sintering Atmosphere	Hardness kg/mm^2	Toughness MPa $\sqrt{m}$	Class
1725°C	6 Hrs	N$_2$	1618	6.42	I
1725°C	14 Hrs	Ar	1580	6.18	II
1775°C	6 Hrs	Ar	1616	6.89	I
1775°C	14 Hrs	N$_2$	1572	6.53	I

Table 4.21 Contribution of Sintering Parameters
in the First Factorial DOE in the Process Optimization

Sintering Parameter	Contribution on Hardness	Contribution on Toughness
Temperature	1.5%	64%
Duration	98%	34%
Atmosphere	0.5%	2%

4.4.3 The Second Two-level Factorial Design of Experiment for Process Optimization

The previous two sets of experiments provided some guidelines for selecting sintering conditions. However, there was a conflict regarding sintering time on fracture toughness. The isothermal experiments suggested that a long sintering time was beneficial to fracture toughness, due to the grain size effect; whereas, the first factorial design of experiment recommended a short sintering time. The second factorial design of experiment was intended to fine-tune the sintering conditions. This DOE also included four sintering runs, all at the same temperature (1775°C). Hardness and

fracture toughness of all HIPed materials were measured, as listed in Table 4.22. ANOVA indicated a strong influence of sintering time on fracture toughness and a significant influence of heating rate on hardness. The contributions of these parameters are listed in Table 4.23. This set of the experiments indicated an advantage to long sintering time (16 Hrs) and slow heating rate (150°C/Hr).

Table 4.22. Hardness and Fracture Toughness of Specimens for the Second Factorial DOE in the Process Optimization

	Gas	Sintering Time Hrs	Heating Rate	Hardness kg/mm^2	Toughness MPa√m	Class
1	N$_2$	16	Fast 500°C/Hr	1556	6.19	I
2	N$_2$	10	Slow 150°C/Hr	1640	5.67	II
3	Ar	16	Slow 150°C/Hr	1639	6.33	I
4	Ar	10	Fast 500°C/Hr	1586	5.80	II

Table 4.23 Contribution of Sintering Parameters in the Second Factorial DOE in the Process Optimization

Sintering Parameter	Contribution on Hardness	Contribution on Toughness
Atmosphere	4 %	6 %
Duration	5 %	94 %
Heating Rate	91 %	0 %

Combining these three sets of experiments, the optimal sintering conditions were decided to be 1775°C for 14 Hrs with a slow heating rate. We also demonstrated that the optimal sintering conditions allowed a low temperature HIPing for the fabrication of Class I silicon nitride.

4.5   Bearing Blank Fabrication and Material Characterization

The composition for the bearing material has been down-selected as 6/0/1/6 (6% Y_2O_3, 1% TiO_2 and 6% AlN). The fabrication of the bearing blanks includes seven unit processes: powder blending, cold isostatic pressing, prenitriding, green machining, nitriding, sintering and hot isostatic pressing, as described in Section 2.0. The program deliverables, 20 RCF and 100 ball bearing blanks, were fabricated and submitted in April 1995. Microstructure, hardness, and fracture toughness were examined, and the results confirmed that the optimized material had Class I properties.

4.5.1 Properties of the Optimized Bearing Material

Selective properties were measured, as listed in Table 4.24. More than one testing laboratory performed the tests. It is not unusual to have different measured data from different laboratories, or using different testing techniques. Overall, the silicon nitride bearing blanks had good hardness, toughness, and flexural strength. R-curve analysis was performed using a controlled flaw bending technique, in which surface flaws were introduced using Vickers indentation at different loadings[9]. Results indicated that the material exhibited a rising R-curve behavior, as shown in Figure 4.31.

Table 4.24 Properties of the Final Deliverables

| Property	Testing Method		Testing Lab
Hardness kg/mm^2	Vickers Indentation	1630	Cercom
Toughness MPa√m	Indentation	6.5	Cercom
Hardness kg/mm^2	Vickers Indentation	1580	UCSB
Toughness MPa√m	Indentation	6.5	UCSB
Toughness MPa√m	Controlled Flaw Bending	5.9	UCSB
Toughness MPa√m	Chevron Notch Bending	6.6	UCLA
Flexural Strength MPa	Four Point Bending	615	UCSB
Flexural Strength MPa	Four Point Bending	764	UCLA
Elastic Modulus GPa	Compressive Testing	275	UCSB
Poissons Ratio	Compressive Testing	0.24	UCSB
Thermal Diffusivity cm^2/s	Laser Flash Technique	0.0822	VPI
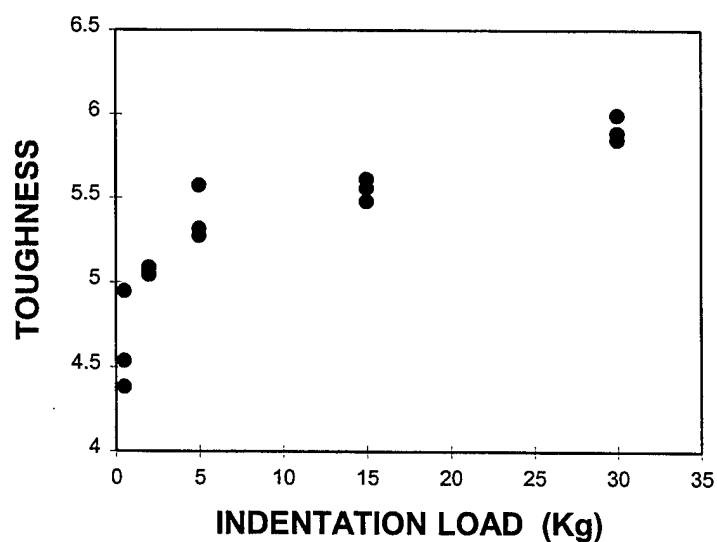
Figure 4.31   *Relationship Between Fracture Toughness (in MPa√m) and Indentation Loading using the Controlled Flaw Bending Technique.*

Failure analysis on selected flexural specimens was performed. Various defects, such as inclusions, glassy agglomerates, and grinding damage, were identified. Figure 4.32 is a micrograph, showing a 100 μm defect. The defect consisted of several large grains, fractured transgranularly. EDX indicated that this region contained Y, Si and Al.

75

Raman analysis was performed, and the result suggested Y_2O_3 inclusions, due to a strong peak centered at 729 cm^{-1}, as shown in Figure 4.33.
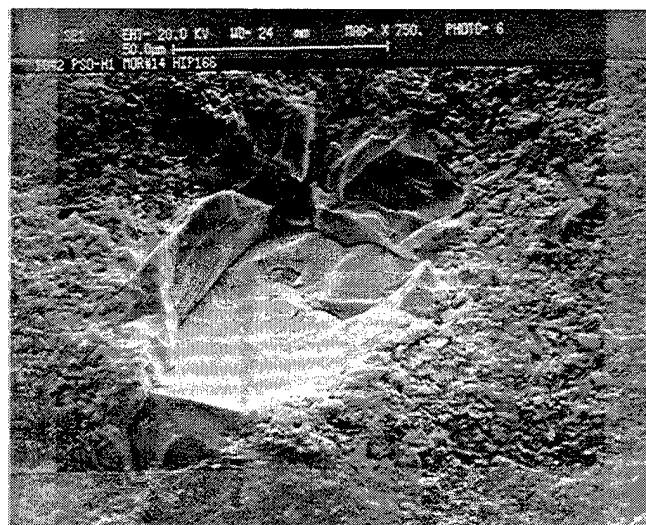

Figure 4.32 Micrograph of Yttrium-rich Inclusions.
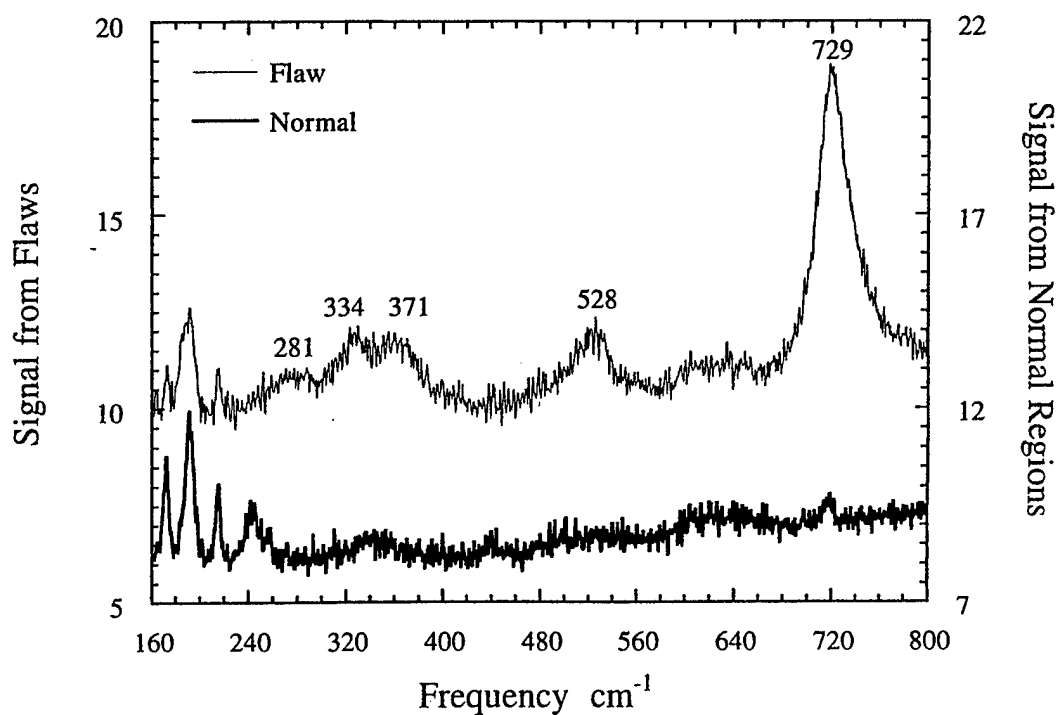

Figure 4.33. Raman Spectra of the Inclusions Shown in Figure 4.32.

Figure 4.34 is a micrograph of another type of inclusion. This defect, known as an inclusion cluster, was about 40 μm in diameter, with EDX detecting only Si. We suspected that there were SiC particles. Glassy agglomerates were also observed, as shown in Figure 4.35. This type of defect could be attributed to an inefficient powder blending process step. The thermal expansion mismatch between these glassy agglomerates and Si_3N_4 caused the cracking.
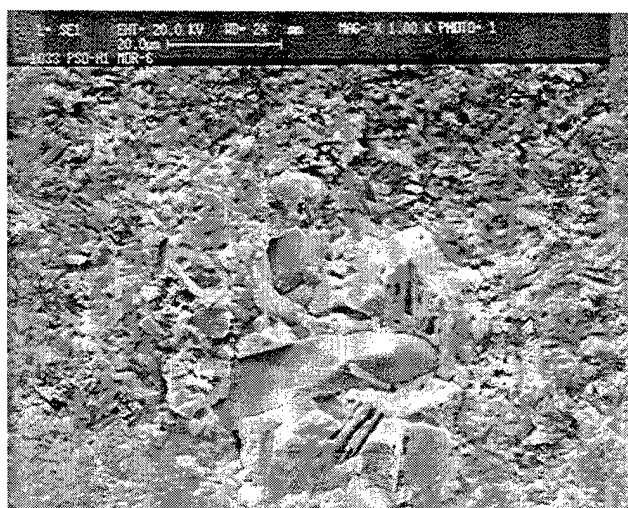

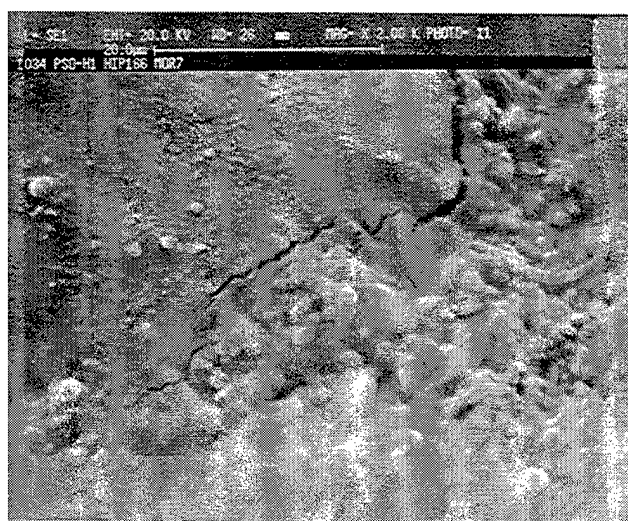**Figure 4.34** Micrograph of Silicon-rich Inclusions.

Figure 4.35 Micrograph of Glassy Agglomerates.

Figure 4.36 shows a surface gouge (grinding damage), about 100 μm long and 5 μm deep. Subsurface damage, generated during diamond grinding, is usually present in ceramic components. Consistent machining procedures must be designed and performed to address the reliability issue related to surface damage.
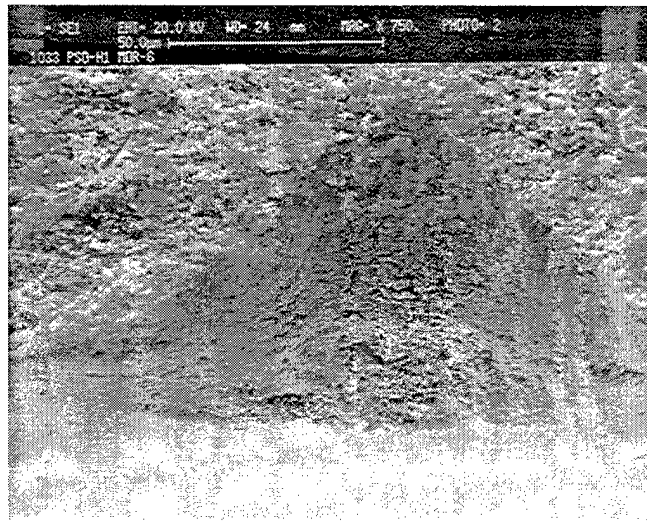

Figure 4.36 Micrograph of Surface Damage.

Results from the failure analysis indicated that powder processing requires further optimization. Powder deagglomeration must be carried out in a contamination-free environment. Final machining must be performed under optimized operational conditions to minimize surface damage.

4.5.2 Microstructure Characterization

Microstructure was examined on polished cross-sections using optical microscopy, as shown in Figure 4.37. The sizes and amounts of porosity, metallic phases, ceramic second phases, and inclusions were within the allowable range for Class I requirements, as shown in Table 4.25.
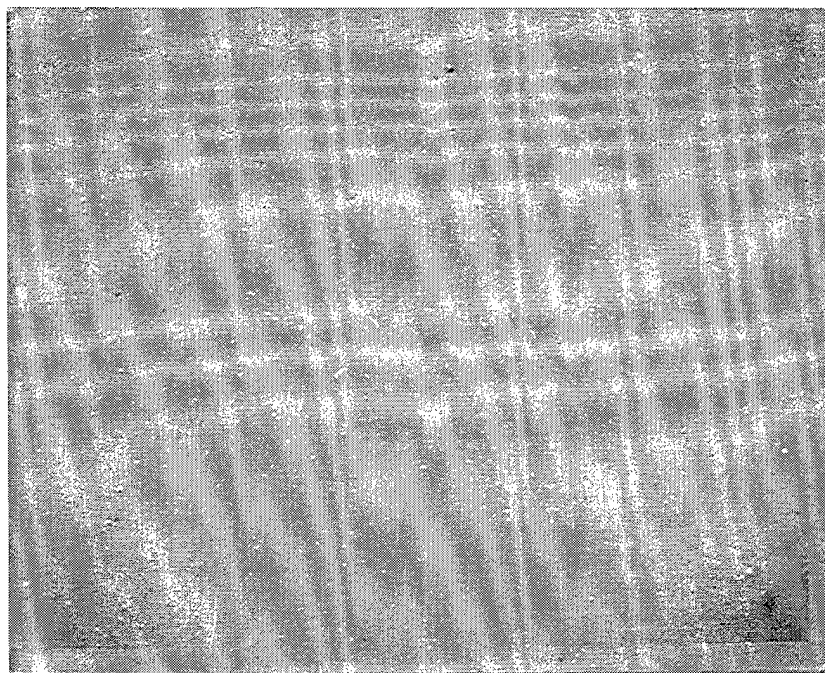
Figure 4.37 Optical Micrograph for the Program Deliverables (200X).

Table 4.25 Microstructure Assessment of the Program Deliverable

		Program Deliverables	Class I Requirement
Porosity	Volume %	0.02	0.02
	Size (μm)	10	10
	Rating	PA02	PA02
Metallic Phases	Volume %	0.06	0.2
	Size (μm)	10	10
	Rating	MA04	MA06
Ceramic Phases	Volume %	0.2	0.2
	Size (μm)	25	25
	Rating	CB06	CB06
Inclusions #/cm²	> 200 μm	0	0
	100 - 200μm	0	0
	50 - 100μm	1	1
	25 - 50μm	3	4

Morphology of Si_3N_4 and distribution of ceramic intergranular phases were examined using scanning electron microscopy, as shown in Figure 4.38. White intergranular phases, light gray stabilized α-Si_3N_4 and dark gray acicular β-Si_3N_4 phases can be identified. Results showed that the acicular β-Si_3N_4, equiaxed stabilized α-Si_3N_4 and intergranular phases were uniformly distributed. A thin surface layer was found in the bearing blanks, as shown in Figure 4.39. The thickness was only about 30 μm, which should not affect the bearing performance, since the subsequent bearing machining (lapping and polishing) can remove this layer. Macrostructure was examined using unaided eyes and stereomicroscopy at low magnification. The macrostructure appearance was uniform, as shown in Figure 4.40.

After this extensive characterization, we concluded that the delivered bearing blanks were a Class I bearing material. This add-on program had successfully developed a composition/process for the fabrication of a Class I material.

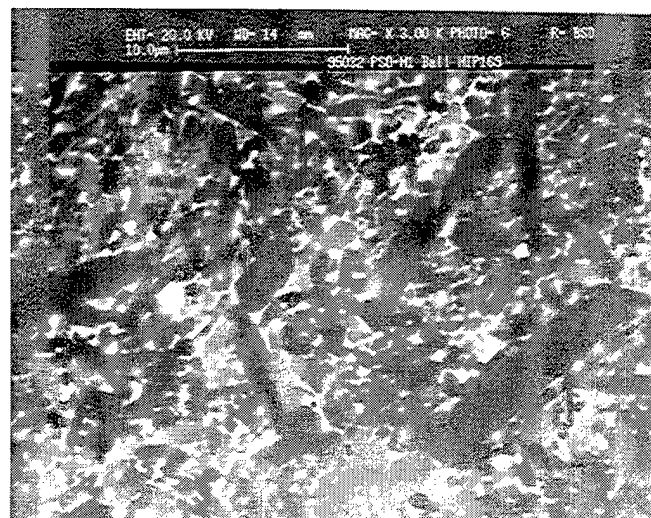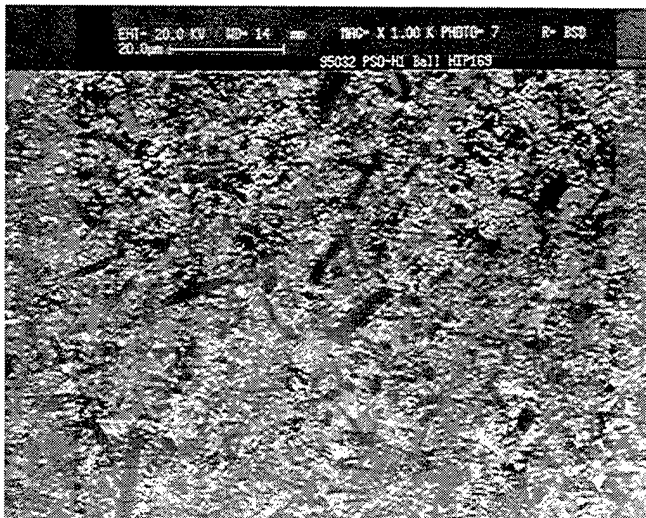1000X   3000X

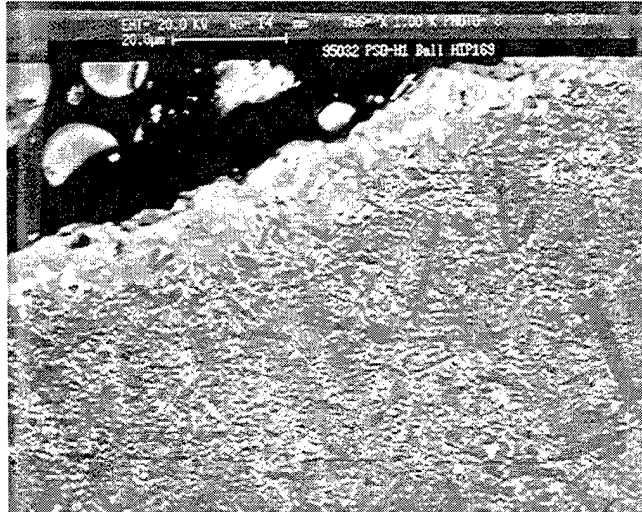

Figure 4.38 SEM Micrographs for the Program Deliverables.

80

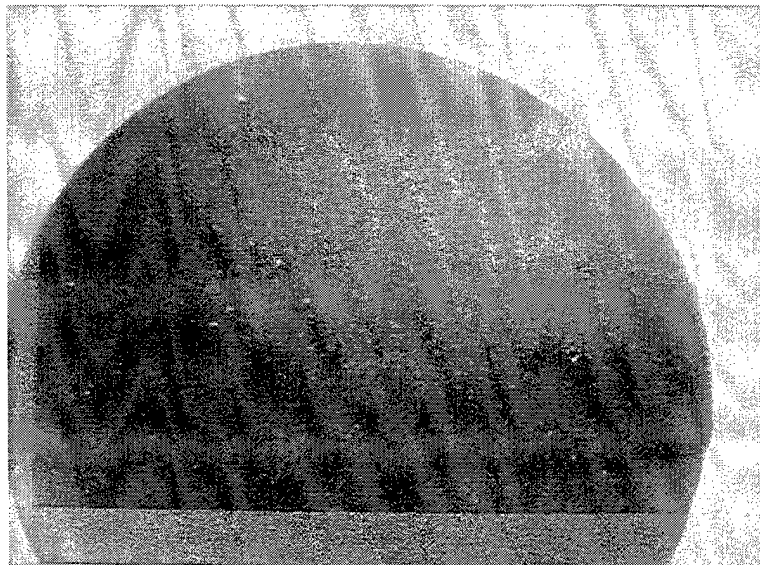*Figure 4.39*   *SEM Micrograph Showing A Surface Layer.*

Figure 4.40   *Macrostructure Appearance of the Program Deliverables (6X).*

4.5.3 Defective Material for Evaluation

One lot of defective ball blanks was submitted for evaluation. This lot of material went through the same powder blending, cold isostatic pressing, prenitriding, green machining, nitriding and sintering as the program deliverables (20 RCF and 100 ball blanks). However, this lot of defective material underwent a separate HIPing run using the same temperature-pressure-time cycle as the program deliverables. The defective balls had a green surface, suggesting formation of SiC, and their macrostructure was not uniform, as shown in Figure 4.41. Fine microporosity caused the material to appear mottled. SEM analysis also indicated that there was a surface reaction, leading to exaggerated grain growth, as shown in Figure 4.42. Intergranular phases seemed to have evaporated close to the surface.

The causes and effects for the microporosity and the mottled appearance are not clear. It is believed that the make-up environment in the furnace was contaminated. In addition, the nitrogen partial pressure did not appear to be sufficient to prevent Si_3N_4 decomposition to SiC. Instead of using N_2/Ar mixed gas, the furnace was initially purged and partially pressurized using N_2 before switching to Ar. The HIP furnace was designed to operate at the range of 140 to 210 MPa (20,000 to 30,000 psi). The initial N_2 pressure (1.75 MPa [250 psi]) is so low that the HIP furnace requires an experienced operator to control precisely. However, we rely on a toll service for the bearing fabrication, resulting in this lot-to-lot variation.
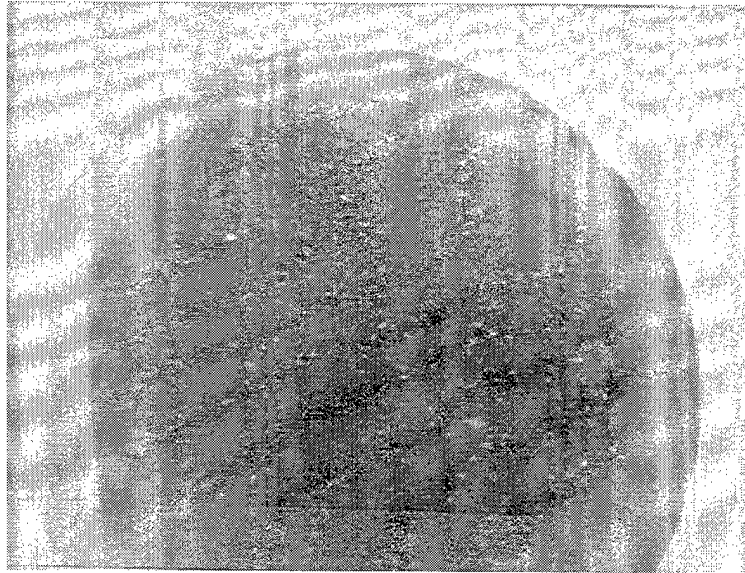
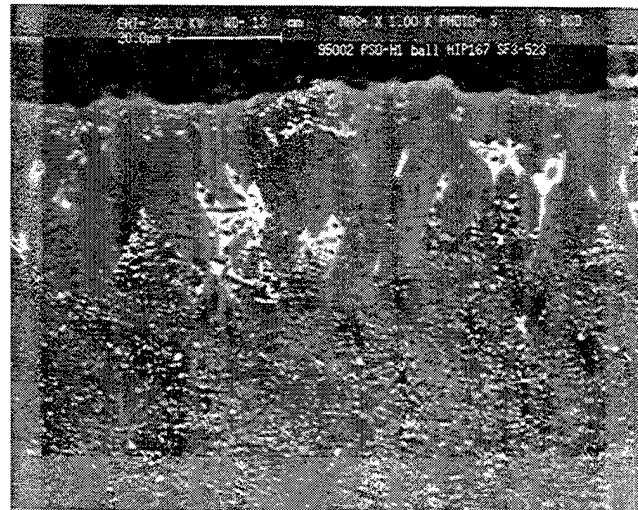**Figure 4.41**   Macrostructure Appearance of the Defective Material (6X).

Figure 4.42   SEM Micrograph Showing a Reaction Layer in the Defective Material
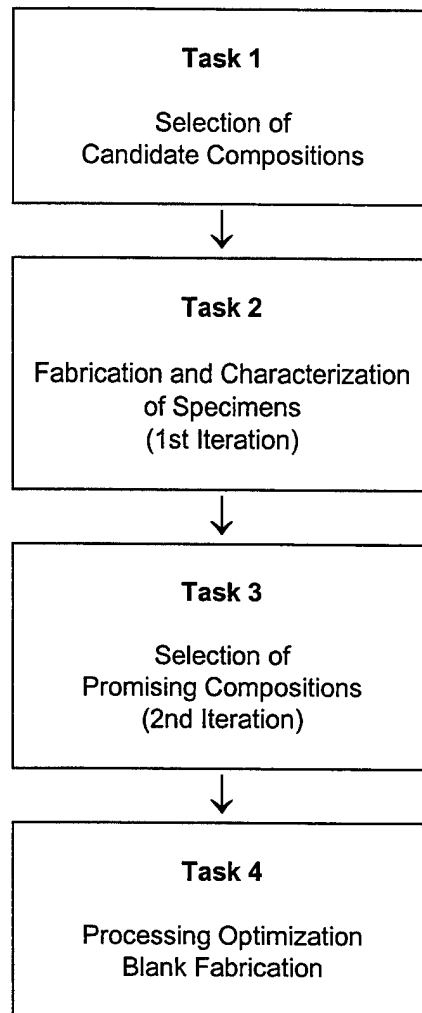
83

BLANK PAGE

5. SUMMARY

This document details the work performed in the "Add-On" portion of a program entitled "Ceramic Bearing Specimen Technology." The objective of the original program was to develop a processing technology capable of producing high-quality ceramic bearing balls at a high production rate and at a competitive cost. The results of the original program were described in the interim report (WL-TR-95-4083). The original program successfully achieved its objectives and the opportunity to further improve the technology was apparent from some of the experimental findings. Additional funding was granted to extend the program for optimizing silicon nitride ceramic ball and rolling contact fatigue specimen blanks. The add-on program was entitled "Optimized Ceramic Bearing Technology."

The objective of the add-on program described in this report was to develop a silicon nitride bearing material with improved hardness and fracture toughness to enhance friction and wear performance, using a high-rate low-cost process, involving reaction bonding, pressureless sintering, and containerless hot isostatic pressing. The program applied an optimization in composition and microstructure to achieve both high hardness and high fracture toughness.

The objective of the add-on program has been successfully met.

The program was divided into four tasks, involving selection of candidate composition, two composition iterations and a processing optimization, as shown in the following flow chart.

```
┌─────────────────────────────┐
│           Task 1            │
│                             │
│        Selection of         │
│    Candidate Compositions   │
└─────────────────────────────┘
               │
               ↓
┌─────────────────────────────┐
│           Task 2            │
│                             │
│  Fabrication and Characterization │
│        of Specimens         │
│        (1st Iteration)      │
└─────────────────────────────┘
               │
               ↓
┌─────────────────────────────┐
│           Task 3            │
│                             │
│        Selection of         │
│    Promising Compositions   │
│        (2nd Iteration)      │
└─────────────────────────────┘
               │
               ↓
┌─────────────────────────────┐
│           Task 4            │
│                             │
│    Processing Optimization  │
│        Blank Fabrication    │
└─────────────────────────────┘
```

All available literature data were reviewed. We analyzed the data in the original program and derived a hardness-composition model to use as a guideline for the experimental matrix. During the first composition iteration, 25 compositions were evaluated using four different processing conditions. In the second composition iteration, an additional 11 compositions were examined, using four different processing conditions. The final composition was selected as 6% Y_2O_3, 1% TiO_2 and 6% AlN (6/0/1/6). Three sets of experimental matrices were performed to optimize the processing conditions for the final down-selected composition. The optimum process was to pressureless sinter at 1775°C and containerless HIP at 1825°C. The new

material is designated as CERCOM PSO-H1, a silicon nitride satisfying the Class I bearing requirements.

The characteristics of the CERCOM PSO-H1 are listed as follows:

Density	3.27 g/cm^3
Hardness	1600 kg/mm^2
Toughness	6.5 MPa $\sqrt{m}$
Flexural Strength	760 MPa
Elastic Modulus	275 GPa
Poissons Ratio	0.24
Thermal Diffusivity	0.082 cm^2/s

CERCOM PSO-H1 has an outstanding combination of high hardness and high fracture toughness. The material consists of "hard" stabilized α-Si$_3$N$_4$ and "tough" acicular β-Si$_3$N$_4$ phases. During sintering and HIPing, α-Si$_3$N$_4$ stabilization, $\alpha \rightarrow \beta$ transformation and β-Si$_3$N$_4$ acicular grain growth processes occur concurrently. Through the composition and process optimization, we have learned how to design and to develop an optimum microstructure to achieve required hardness and fracture toughness. The successful development of PSO-H1 makes Class I bearing blanks available for the first time in the United States.

BLANK PAGE

6. REFERENCES

1. R. N. Katz, "Silicon Nitride: An Ongoing Example of Advanced Ceramics Development," Interceram, 41 [4] (1991), 231-256.

2. N. Ingelstroem and T. Ekstroem, "Silicon Nitride Made by the Encapsulated HIP Technique", Proceedings of the International Conference on Hot Isostatic Pressing, (1987), 307-314.

3. R. E. Loehman, "Oxynitride Glasses," Treatise on Materials Science and Technology, vol. 26 (1985), 119-149.

4. A. K. Mukhopadhyay, S. K. Datta and D. Chakraborty, "On the Microhardness of Silicon Nitride and Sialon Ceramics," J. of the European Ceramic Society, 6 (1990), 303-311.

5. T. Kawashima, H. Okamoto, H. Yamamoto and A. Kitamura, "Grain Size Dependence of the Fracture Toughness of Silicon Nitride Ceramics," J. of the Ceramic Society in Japan, 99 [4] (1991), 320-323 (in Japanese).

6. E. M. Knutson-Wedel, L. K. L. Falk, H. Bjoerklund and T. Estroem, "Si_3N_4 Ceramics Formed by HIP using Different Oxide Additions - Relation Between Microstructure and Properties," J. Mat. Sci., 26 (1991), 5575-5584.

7. K. R. Lai, T. Y. Tien, "Kinetics of β Si_3N_4 Grain Growth in Si_3N_4 Ceramics Sintered under High Nitrogen Pressure," J. Am. Ceram. Soc., 76 [1] (1994), 91-96.

8. M. J. Hoffmann and G. Petzow, "Microstructural Design of Si_3N_4 Based Ceramics," in Silicon Nitride Ceramics, Material Research Society Symposium Proceedings, Vol. 287, (1993), 3-14.

9. P. Chantikul, G. R. Antis, B. R. Lawn and D. B. Marshall, "A Critical Evaluation of Indentation Techniques for Measuring Fracture Toughness: II Strength Method," J. Am. Ceram. Soc., 64 [9] (1981), 539-43.